Boundary-Layer Meteorol (2011) 139:307–332
DOI 10.1007/s10546-010-9586-9

ARTICLE

Critical Evaluation of Scalar Roughness Length Parametrizations Over a Melting Valley Glacier

Xiaofeng Guo · Kun Yang · Long Zhao · Wei Yang · Shenghai Li · Meilin Zhu · Tandong Yao · Yingying Chen

Received: 23 June 2010 / Accepted: 30 December 2010 / Published online: 15 January 2011

Abstract We present a field investigation over a melting valley glacier on the Tibetan Plateau. In the ablation zone, aerodynamic roughness lengths (z_{0M}) vary on the order of 10^{-4}–10^{-2} m, whose evolution corresponds to three melt phases with distinct surface cover and moisture exchange: snow (sublimation/evaporation), bare ice (deposition/condensation), and ice hummocks (sublimation/evaporation). Bowen-ratio similarity is validated in the stably stratified katabatic winds, which suggests a useful means for data quality check. A roughness sublayer is regarded as irrelevant to the present ablation season, because selected characteristics of scalar turbulence over smooth snow are quite similar to those over hummocky ice. We evaluate three parametrizations of the scalar roughness lengths (z_{0T} for temperature and z_{0q} for humidity), viz. key factors for the accurate estimation of sensible heat and latent heat fluxes using the bulk aerodynamic method. The first approach is based on surface-renewal models and has been widely applied in glaciated areas; the second has never received application over an ice/snow surface, despite its validity in (semi-)arid regions; the third, a derivative of the first, is proposed for use specifically over rough ice defined as $z_{0M} > 10^{-3}$ m or so. This empirical z_{0M} threshold value is deemed of general relevance to glaciated areas (e.g. ice sheet/cap and valley/outlet glaciers), above which the first approach gives notably underestimated $z_{0T,q}$. The first and the third approaches tend to underestimate and overestimate turbulent heat/moisture exchange, respectively, frequently leading to relative errors higher than 30%. Comparatively, the second approach produces fairly low errors in energy flux estimates both in individual melt phases and over the whole ablation season; it thus emerges as a practically useful choice to parametrize $z_{0T,q}$ in glaciated areas. Moreover, we find all

X. Guo (✉) · K. Yang · L. Zhao · W. Yang · S. Li · M. Zhu · T. Yao · Y. Chen
Key Laboratory of Tibetan Environment Changes and Land Surface Processes, Institute of Tibetan Plateau Research, Chinese Academy of Sciences, Beijing 100085, People's Republic of China
e-mail: hsiaofengguo@gmail.com

K. Yang
e-mail: yangk@itpcas.ac.cn

L. Zhao · S. Li · M. Zhu
Graduate University of Chinese Academy of Sciences, Beijing 100049, People's Republic of China

three candidate parametrizations unable to predict diurnal variations in the excess resistances to humidity transfer, thus encouraging more efforts for improvement.

Keywords Bowen-ratio similarity · Bulk aerodynamic method · Eddy-covariance method · Katabatic wind · Scalar roughness length · Stable boundary layer

1 Introduction

Glaciated areas provide an ideal laboratory to study the stable atmospheric boundary layer, mainly because of several surface features (cf. Andreas 2002; Heinemann 2008; Vihma et al. 2009). For example, the temperature of a melting ice/snow surface is normally very close to 273 K, which exhibits rather insignificant variations compared with that of common land surfaces; saturation vapour pressure can be assumed close to the ice/snow–atmosphere interface. An optimally homogeneous underlying surface is thus available.

Katabatic winds are characteristic of the air motion over a glaciated surface; hence the term 'glacier wind' that is jointly driven by downward sensible heat transport in the stable boundary layer and the radiative cooling on a sloping terrain (cf. Chiba and Kobayashi 1986; Oerlemans and Grisogono 2002; Parish and Cassano 2003; Anderson and Neff 2008). A wind speed maximum (low-level jet) is often present in the katabatic flow, normally found in a thin layer close to the ice/snow surface (roughly 10 m or thinner; e.g. Forrer and Rotach 1997; Oerlemans et al. 1999; Denby and Snellen 2002). Significant wind shear induced by the elevated jet generates continuous turbulence that efficiently transports momentum and scalars (e.g. Heinemann 2004; Parmhed et al. 2004), though a strong temperature inversion commonly exists with a positive lapse rate of about 1 K m^{-1} (e.g. Munro and Davies 1978; Pasricha et al. 1991; Oerlemans 2001; Hudson and Brandt 2005). The validity of Monin–Obukhov similarity theory, therefore, is restricted by the jet's existence and resultant vertical flux divergence (Oerlemans and Grisogono 2002). Relevant techniques to estimate turbulent fluxes, such as the bulk aerodynamic method widely used in glacio-meteorological investigations, should be usable only within the lowest several metres above the surface (e.g. Munro and Davies 1977, 1978; Denby and Greuell 2000; Andreassen et al. 2008; Oerlemans 2010). As Hock (2005) argued, the determination of turbulent fluxes still constitutes a major uncertainty in energy-balance melt models, partly due to potential errors in the scalar roughness length parametrization. Critical evaluations against eddy-covariance turbulence data are truly necessary (e.g. Munro 1989; cf. Andreas 2002).

In a katabatic flow, turbulent sensible heat and latent heat fluxes are significant components of the heat and moisture budgets, respectively (van den Broeke 1997a); both types of heat flux can also be important sources of a glacier's melt energy. Their total contribution typically ranges from 25 to 50%, depending on the surface albedo, synoptic conditions, and climatic region (e.g. Bintanja 1995; van den Broeke 1997b; van den Broeke et al. 2008; Oerlemans et al. 1999; van der Avoird and Duynkerke 1999; Oerlemans and Klok 2002; Klok et al. 2005; Giesen et al. 2008, 2009; Konya and Matsumoto 2010). Besides, moisture exchange is a component inherent in the mass budget. For instance, Stössel et al. (2010) directly observed the link between the turbulent deposition of water vapour and the growth of hoar crystals over a snow surface. Turbulent mechanisms underlying the glacier's energy and mass budgets, therefore, are of particular concern in glacio-meteorological measurements and mass balance modelling (cf. Oerlemans 1998; Greuell and Genthon 2004; Munro 2006).

As far as parametrization is concerned, various schemes rely on roughness lengths for momentum (z_{0M}) and scalars to predict turbulent fluxes (cf. Cassano et al. 2001). While

z_{0M} is closely related to surface morphology, scalar roughness lengths usually need to be parametrized. For example, based on surface-renewal models, Andreas (1987) proposed original formulations to parametrize the roughness lengths for temperature (z_{0T}) and humidity (z_{0q}). These have been extensively adopted for energy budget measurements or modelling in glaciated areas (cf. Andreas 2002; e.g. Klok et al. 2005; van den Broeke et al. 2006, 2008; Giesen et al. 2008). Critical evaluations, however, are still limited. One early effort was concerned with aerodynamically smooth flow over Antarctic blue ice and snow, where snow-drift processes rendered z_{0M} quite variable (Bintanja and van den Broeke 1995). A reasonable agreement with Andreas's (1987) model of z_{0T} was seen over the highly smooth ice (viz. $z_{0M} \sim 10^{-6}$ m). Denby and Snellen (2002) found that z_{0T} predictions using Andreas's (1987) model were well consistent with profile-based estimates over a melting valley glacier. Andreas (2002) collected extensive datasets over both snow and ice surfaces; although the datasets of different origin led to mixed results, Andreas's (1987) model of z_{0T} generally gained support in various aerodynamic flow regimes. Continued examinations were mostly devoted to relatively smooth surfaces such as snow-covered sea-ice in separate seasons, where z_{0M} values typically lay between 10^{-5} and 10^{-3} m; Andreas's (1987) models of both z_{0T} and z_{0q} agreed with gradient-based retrievals overall (e.g. Andreas et al. 2004, 2005a,b, 2010a,b; Brunke et al. 2006). Using a composite dataset covering a wide range of z_{0M} values (i.e. 10^{-5}–10^{-1} m), Smeets and van den Broeke (2008b) had a novel finding: Andreas's (1987) model resulted in systematically underestimated sensible heat and latent heat fluxes (absolute values) over rough ice, particularly evident when z_{0M} exceeded 10^{-3} m or so (7×10^{-4} m to be exact). Although this z_{0M} threshold value is empirical, it led to an interesting argument: a roughness sublayer should develop over the ice hummocks, where scalars were transported more efficiently than predicted by Andreas (1987), who omitted the potential effects of the roughness sublayer. Efforts to evaluate the z_{0q} parametrization are relatively few, but rewarding: '…, we need to concentrate on making the measurements required for evaluating z_{0q}' (Andreas 2002).

Our study seeks to critically evaluate three physical $z_{0T,q}$ parametrizations for energy flux estimations using the bulk aerodynamic method. We organise the paper as follows: Sect. 2 presents the bulk aerodynamic method and three candidate parametrizations of $z_{0T,q}$; in Sect. 3, we introduce a short-term field experiment over a melting valley glacier on the Tibetan Plateau, as well as eddy-covariance flux corrections and glacio-meteorological characteristics. Section 4 is devoted to the results and relevant discussions, while final remarks and recommendations compose Sect. 5.

2 Theory and Methodology

2.1 Flux Estimations Using the Bulk Aerodynamic Method

The bulk aerodynamic method estimates turbulent fluxes of momentum (τ_{BA}), sensible heat (H_{BA}), and latent heat (LE_{BA}) by introducing the bulk transfer coefficients for momentum (C_D), temperature (C_T), and humidity (C_q), respectively:

$$\tau_{BA} = \rho C_D \overline{U}^2, \tag{1}$$

$$H_{BA} = \rho c_p C_T \overline{U}(\overline{\theta}_0 - \overline{\theta}_A) = \rho c_p C_T \overline{U} \Delta\overline{\theta}, \tag{2}$$

$$LE_{BA} = \rho \lambda C_q \overline{U}(\overline{q}_0 - \overline{q}_A) = \rho \lambda C_q \overline{U} \Delta\overline{q}, \tag{3}$$

where ρ is the air density, c_p is the specific heat capacity of air (1,005.7 J kg^{-1} K^{-1}), λ is the latent heat for moisture exchange: $\lambda = 2.834 \times 10^6$ J kg^{-1} for sublimation/deposition and $\lambda = 2.501 \times 10^6$ J kg^{-1} for evaporation/condensation, $\overline{U}$ is the mean wind speed, $\overline{\theta}_m$ and $\overline{q}_m$ are mean potential temperature and specific humidity, respectively (the subscript m represents a medium, namely '0' for the surface or 'A' for the air), leading to the surface-air differences defined as $\Delta\overline{\theta} = \overline{\theta}_0 - \overline{\theta}_A$ and $\Delta\overline{q} = \overline{q}_0 - \overline{q}_A$. To differentiate between sublimation/deposition and evaporation/condensation processes, we assume that evaporation/condensation occurs when $\overline{\theta}_0$ exceeds 273.15 K, since liquid water may be continuously present on the surface; and, sublimation/deposition occurs when $\overline{\theta}_0 < 273.15$ K (see DeWalle and Rango 2008). The heat-flux sign convention is: negative sensible heat fluxes indicate surface-directed heat transport in the stably stratified boundary layer; positive and negative latent heat fluxes denote upward (sublimation/evaporation) and downward (deposition/condensation) transport of water vapour, respectively.

Letting z_M, z_T, and z_q denote the reference heights of $\overline{U}$, $\overline{\theta}_A$, and $\overline{q}_A$, respectively, C_D, C_T, and C_q are deduced from Monin–Obukhov similarity theory (cf. Garratt 1992):

$$C_D = \frac{\kappa^2}{\left[\ln\left(\frac{z_M}{z_{0M}}\right) - \Psi_M\left(\frac{z_M}{L}\right)\right]^2}, \tag{4}$$

$$C_s = \frac{\kappa^2}{\left[\ln\left(\frac{z_M}{z_{0M}}\right) - \Psi_M\left(\frac{z_M}{L}\right)\right]\left[\ln\left(\frac{z_s}{z_{0s}}\right) - \Psi_s\left(\frac{z_s}{L}\right)\right]}, \tag{5}$$

where κ is the von Kármán constant (0.4), L is the Obukhov length, the subscript s in Eq. 5 represents a specific scalar, namely 'T' for temperature or 'q' for humidity, Ψ_M and Ψ_s are the stability correction functions for wind velocity and scalar, respectively. We adopt the Ψ_M and Ψ_T formulations from Holtslag and de Bruin (1988) in the stable boundary layer, as well as the normal assumption $\Psi_q = \Psi_T$ (see, for example, Forrer and Rotach 1997 for detailed evaluations in katabatic flow, and Andreas 2002 for recommendations). In fact, the stability corrections Ψ_M and Ψ_s have rather weak effects in Eqs. 4 and 5, primarily owing to the relatively low measurement heights herein (i.e. z_M, z_T, and z_q). Eddy-covariance measurements in our case show that L is typically on the order of tens of metres with a median value of 47 m. The non-dimensional stability parameter ($\zeta = z_{M,s}/L$) is thus very low, making values of both Ψ_M and Ψ_s close to zero. The choice of their functional forms, therefore, should be less of a concern in our study, due to their insignificant effect on flux estimations overall.

As evident in Eqs. 4 and 5, one primary cause of the difference between C_D and C_s is the inequality between z_{0M} and z_{0s}, thus introducing the 'excess resistance to scalar transfer', viz. $\kappa B^{-1} = \ln(z_{0M}/z_{0T})$ for temperature and $\kappa A^{-1} = \ln(z_{0M}/z_{0q})$ for humidity (cf. Garratt 1992). Both κB^{-1} and κA^{-1} values are typically positive, since the relation $z_{0M} > z_{0T,q}$ generally holds. In essence, momentum is more efficiently transferred due to pressure drag around individual roughness elements, while scalar transport is strongly governed by molecular diffusion close to the surface—the 'bluff-body effect', one dominant mechanism that affects κB^{-1} (or κA^{-1}; cf. Haverd et al. 2010).

To apply the bulk aerodynamic method, we regard z_{0M} as an input variable whose value can be 'retrieved' from Eqs. 1 and 4 (see also Eq. 6) by using eddy-covariance turbulence data and gradient measurements (details to be introduced in Sect. 3.1). Then, z_{0T} and z_{0q} are parametrized using three different candidate formulations (see Sect. 2.2). Equations 1–5 are solved by numerical iteration to deduce the required turbulence parameters and fluxes. To derive values of z_{0M}, z_{0T}, and z_{0q} directly from the dataset, we first calculate C_D, C_T, and

C_q based on bulk formulations of Eqs. 1, 2 and 3, respectively, viz. $C_D = \tau_{EC}/(\rho\overline{U}^2)$, $C_T = H_{EC}/(\rho c_p \overline{U}\Delta\overline{\theta})$, and $C_q = LE_{EC}/(\rho\lambda\overline{U}\Delta\overline{q})$, where τ_{EC}, H_{EC}, and LE_{EC} are eddy-covariance flux measurements. Then, z_{0M} and $z_{0T,q}$ are solved by re-arranging Eqs. 4 and 5, respectively (see also, for example, Andreas et al. 2005a, 2010a,b):

$$z_{0M} = z_M \exp\left\{-\left[\kappa C_D^{-1/2} + \Psi_M\left(\frac{z_M}{L}\right)\right]\right\}, \tag{6}$$

$$z_{0s} = z_s \exp\left\{-\left[\kappa C_D^{1/2} C_s^{-1} + \Psi_s\left(\frac{z_s}{L}\right)\right]\right\}, \tag{7}$$

where the subscript s still denotes *scalar* and is replaced by 'T' for temperature or 'q' for humidity. Roughness lengths as computed above are referred to as 'retrieved' values herein, as well as their derivatives such as κB^{-1} and κA^{-1}.

2.2 Sampling of Scalar Roughness Length Parametrizations

We focus on three physical parametrizations for critical evaluation; they originate from Andreas (1987), Yang et al. (2002), and Smeets and van den Broeke (2008b), which are referred to, respectively, as the A87, Y02, and SvdB approaches hereafter.

Originally calibrated using datasets over snow and sea-ice, the A87 approach is widely applied in glaciated areas (e.g. ice sheet and valley glacier). Andreas (1987) established the interfacial-sublayer profiles of scalars based on surface-renewal models, before matching the profiles with those in the constant-flux layer where flux-gradient relations apply. A87 expresses $\ln(z_{0s}/z_{0M})$ (i.e. $-\kappa B^{-1}$ and $-\kappa A^{-1}$) in terms of the roughness Reynolds number ($Re_* \equiv u_* z_{0M}/\nu$, where u_* is the friction velocity, and ν is the kinematic viscosity of air):

$$\ln(z_{0s}/z_{0M}) = b_0 + b_1 \ln(Re_*) + b_2[\ln(Re_*)]^2, \tag{8}$$

where values of the polynomial coefficients $b_{0,1,2}$ depend on the aerodynamic flow regime. Table 1 gives their values for rough flow ($2.5 \le Re_* \le 1000$) concerned herein, where the values of $b_{0,1,2}$ distinguish between z_{0T} and z_{0q}.

The SvdB approach is a derivative of A87; with a new set of coefficients in Eq. 8 (see Table 1); SvdB is intended for use specifically over rough ice (i.e. $z_{0M} > 10^{-3}$ m as an empirical threshold value suggested in Smeets and van den Broeke 2008b). To explain the notably underestimated heat and moisture exchange by the A87 approach when z_{0M} exceeds 10^{-3} m, Smeets and van den Broeke (2008b) argue that a roughness sublayer should develop at relatively high z_{0M} values, where turbulent transfer of scalars is possibly enhanced. The SvdB approach thus predicts higher $z_{0T,q}$ values than A87, leading to an increased level of turbulent exchange.

The Y02 approach is proposed over bare-soil surface and has never been applied in glaciated areas. By drawing an analogy between natural flow and that over a smooth flat plate,

Table 1 Values of the polynomial coefficients $b_{0,1,2}$ in Eq. 8 to parametrize the scalar roughness lengths

Reference	Scalars	b_0	b_1	b_2
Andreas (1987)	Temperature (T)	0.317	−0.565	−0.183
	Humidity (q)	0.396	−0.512	−0.180
Smeets and van den Broeke (2008b)	Temperature and humidity (T, q)	1.500	−0.200	−0.110

Yang et al. (2002) applied knowledge of wall-bounded shear flows, whose feature depends on the non-dimensional height (y^+):

$$y^+ = \frac{hu_*}{\nu}, \tag{9}$$

where h is the height above the surface, y^+ defines three regions in the turbulent boundary layer, i.e. the viscous sublayer, buffer layer, and inertial sublayer (e.g. Davidson 2004). Normally, when y^+ exceeds a lower limit of 40–70, logarithmic wind velocity profiles are applicable (see Townsend 1976). The Y02 approach is innovative in adopting an h value of $h_T = 70\nu/u_*$ to scale z_{0T} by introducing $\kappa K^{-1} = \ln(h_T/z_{0T})$; h_T is probably more meaningful than z_{0M}, which is indeed a fictitious quantity (i.e. the height at which the wind speed goes to zero in the logarithmic profile). By expressing κK^{-1} as a function of two turbulent scales (i.e. u_* and θ_*), Yang et al. (2002) parametrize z_{0T} as ($z_{0q} = z_{0T}$ is assumed here):

$$z_{0T} = h_T \exp\left(-\Omega u_*^{1/2} |\theta_*|^{1/4}\right) \equiv h_T \exp\left(-\Omega u_*^{1/4} \left|\frac{H}{c_p \rho}\right|^{1/4}\right), \tag{10}$$

where u_* is the friction velocity, θ_* is the scaling parameter of temperature, H is the sensible heat flux, and the powers 1/2 and 1/4 are empirically determined to best-fit the experimental coefficient Ω ($7.2\,\mathrm{s}^{1/2}\,\mathrm{m}^{-1/2}\,\mathrm{K}^{-1/4}$). The Y02 approach proves superior to several alternatives in making accurate sensible heat flux estimates in (semi-)arid regions, mainly thanks to its effective modelling of the z_{0T} diurnal variation (e.g. Yang et al. 2008, 2009; Chen et al. 2010). Nonetheless, the usefulness of the Y02 approach is pending in glaciated areas with distinct surface features: a melting ice/snow surface has roughly fixed temperatures, and z_{0M} often exhibits a remarkable evolution during the ablation season (e.g. Smeets et al. 1999; Smeets and van den Broeke 2008a).

3 Glacio-meteorological Experiment and Data Processing

3.1 Site and Measurements

A field experiment was carried out from May 20 to September 9, 2009 at Palong-Zangbu No. 4 Glacier[1] on the south-east Tibetan Plateau. This valley glacier covers an area of about 12.8 km^2 and spans in altitude 4,650–5,800 m (see Xu et al. 2009 for a topographic map). The valley (or snout), generally 700 m wide, is inclined roughly at 5° with its downslope axis oriented towards the north-north-east direction (about 20° from north). Our site was located in the glacier's ablation zone, namely at 4,800 m above sea level (29°15′N, 96°55′E; about 1,500 m away from the glacier front position).

Meteorological instruments included an eddy-covariance system using a CSAT3 three-dimensional sonic anemometer (Campbell Scientific Inc., Logan, Utah, USA) and a LI-7500 open-path gas analyser (Li-Cor Inc., Lincoln, Nebraska, USA). They measured three components of turbulent wind velocity, virtual temperature, and water vapour concentrations; the turbulence raw data were collected at 10 Hz. Also available were CNR1 pyronometers and pyrgeometers (Kipp & Zonen, Delft, The Netherlands), which measured four radiation components. Housed in a radiation shield, a HMP45C temperature and relative humidity

[1] Also known as Parlung No. 4 Glacier.

sensor (Campbell Scientific Inc., Logan, Utah, USA) made auxiliary measurements of the ambient air. Both CNR1 and HMP45C sensors provided half-hourly average values.

All instruments were mounted on a single tripod, but the rapid melt did not allow the tripod to be firmly anchored to the surface. Instead, the tripod was allowed to stand freely on the ice surface, being able to sink along three steel bars drilled into the ice. Hopefully, the sensors could have largely stable reference heights relative to the ice surface. Several photographs of our experimental set-up are available at http://www.sciencenet.cn/u/hsiaofengguo/,[2] where we observe that the surface cover sees a marked evolution during this ablation season (i.e. snow, bare ice, and ice hummocks in chronological order). The ice/snow melt led to substantial darkening of the surface, and ice hummocks and meltwater streams emerged due to differential ice melt. Using height records of nine mass balance stakes, monthly surface melt is quantified as -1.57 ± 0.03 m from June 3 to September 9.

To lessen the problem of vertical flux divergence, the eddy-covariance system was desirably placed close to the surface (see King 1990; Meesters et al. 1997; Oerlemans et al. 1999; Denby and Greuell 2000; Smeets et al. 2000; Stössel et al. 2010). The instruments' reference heights, i.e. vertical distance between a transducer and the ice surface, could not be fixed over the bumpy and unsteady melting ice. For simplicity, we average the records from a total of 14 site visits: the eddy-covariance system has an average height of 1.72 ± 0.12 m above the *local* ice surface, i.e. z_M value for $\overline{U}$ by the CSAT3 transducer. The HMP45C and CNR1 instruments were mounted higher than the eddy-covariance system by 0.6 and 0.4 m, respectively. So, both z_T and z_q values are equal to $z_M + 0.6$ m, viz. for air temperature ($\overline{\theta}_A$) and relative humidity ($\overline{q}_A$) measurements by the HMP45C transducer. Moreover, we correct z_M and $z_{T,q}$ values for use over a melting snow surface, with details given in Sect. 3.2.

The albedo (α) is directly derived from incoming and reflected shortwave radiation measured by the CNR1 instrument; besides, upwelling (R_{Lu}) and downwelling (R_{Ld}) longwave radiation data are used to estimate the surface temperature ($\overline{\theta}_0$), based on:

$$R_{Lu} = (1 - \varepsilon) R_{Ld} + \varepsilon \sigma \overline{\theta}_0^4, \tag{11}$$

where the surface emissivity (ε, equal to the absorptivity) is assumed to be 1.0, so that $\overline{\theta}_0$ values reasonably fluctuate around the melting point of ice (to be illustrated in Fig. 1a); σ is the Stefan–Boltzmann constant (5.67×10^{-8} W m^{-2} K^{-4}). In addition, values of specific humidity ($\overline{q}_0$ and $\overline{q}_A$ in Eq. 3) are readily derived from the saturation vapour pressure (e_{sat}), relative humidity (RH), and atmospheric pressure; e_{sat} values separately for the surface and the ambient air are computed using the Clausius–Clapeyron equation (cf. Tsonis 2002); RH takes the value of 100% for a saturated ice/snow surface.

3.2 Turbulent Flux Corrections and Glacio-meteorological Characteristics

Defensible efforts to evaluate surface flux parametrizations are demanding, not least due to various unresolved issues to ensure the accuracy of eddy-covariance turbulent fluxes (cf. Mahrt 2010). We now proceed with several steps regarding their corrections.

To calculate sensible heat fluxes, we follow Schotanus et al. (1983) to convert the sonic temperature into actual temperature. Eddy-covariance latent heat fluxes involve a 'WPL' correction for density effects (cf. Webb et al. 1980). This correction is presently found to reduce sublimation/evaporation rates by about 7% overall, i.e. a relatively low magnitude similarly found for typical ecosystems (cf. Mauder and Foken 2006). The 'WPL' correction appreciably enhances deposition/condensation rates by nearly 40% overall, possibly as a

[2] See the blog entry entitled 'ITP-CAS Glacio-meteorological Experiment: 2009'.

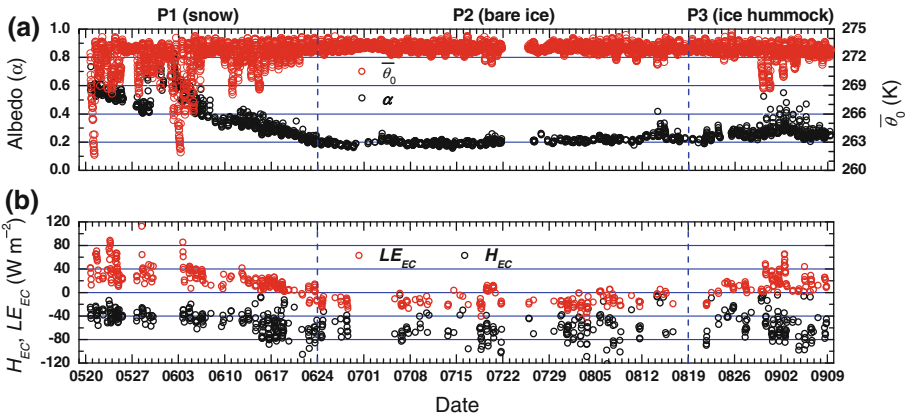

Fig. 1 Time series of half-hourly measurements: **a** mean albedo (α) and surface temperature ($\overline{\theta}_0$), and **b** eddy-covariance turbulent fluxes of sensible heat (H_{EC}) and latent heat (LE_{EC}). Only the quality-controlled data are presented in **b**. The *blue dashed lines* separate the three melt phases (P1, P2, and P3)

result of relatively high Bowen ratios that are mostly above two in the present dataset (see also Liebethal and Foken 2003, 2004).

Previous turbulent flux measurements in glaciated areas seem inclined to adopt bulk averaging for short periods, such as 10 min (e.g. King 1990; King et al. 2006) and 15 min (e.g. Stössel et al. 2010). To determine an adequate averaging period, we examine ogive functions of the momentum and heat fluxes, which show that low-frequency turbulence makes very limited flux contributions overall (figure omitted). We thus use 30-min bulk averaging throughout our study. Moreover, to correct for potential flux loss at high frequencies (possibly caused by path averaging and limited sampling frequency; see Kaimal and Finnigan 1994), we correct raw flux data using the transfer-function technique with the cospectral models of Kaimal et al. (1972) (see Moore 1986 for algorithm). In general, the corrected fluxes (absolute values) are about 3% higher than the raw values.

The natural wind coordinate, as coined in Lee et al. (2004), is then applied with a double-step rotation procedure involving two correction angles (McMillen 1988). Specifically, yaw- and pitch-correction angles are computed from half-hourly measurements of the mean wind vector, which make its lateral and vertical components vanish, respectively (see also Smeets et al. 2000; Smeets and van den Broeke 2008b). Plotting time series of the correction angles (figure omitted), we find it interesting that the 'yaw' angle sees no discernible changes throughout the field campaign, which spans 20°–70° with an average of 45° ± 11°. By contrast, the 'pitch' angle, spanning −8° to 2°, either increases or decreases with time (particularly evident over an ice surface), until the tripod's arm and the eddy-covariance system are subject to a manual re-leveling regularly once a week. These variations in the 'pitch' angle, in fact, point to the fact that an instrument mast/tower can easily be tilted on melting glaciers and thus necessitates frequent site maintenance to guarantee the data quality.

Following Foken et al. (2004), a stationarity test is made for turbulent momentum and heat fluxes. This test mainly rejects fluxes of relatively low magnitude, which typically occur at 0000–1000 local time (LT: UTC plus 7 h). A total of 487 half-hourly eddy-covariance turbulence measurements survive to serve further analysis. As normally observed in glaciated areas, persistent katabatic winds prevail in the present dataset, which lead to a four-month average wind direction of 199° ± 9°, reasonably along the downslope valley axis. The steady

wind direction, plus optimal surface homogeneity, makes the flux footprint less of a concern here. Nonetheless, a sufficient upwind fetch should remain relevant, given the fact that an ice fall marked a sudden transition from the accumulation zone to the ablation zone. In order for turbulent flux measurements to be representative of the ablation zone, we set up the instruments where an upwind fetch of at least 1.5 km is available (i.e. at 4,800 m above sea level).

Figure 1 illustrates time series of the albedo (α), surface temperature ($\overline{\theta}_0$), and eddy-covariance sensible heat (H_{EC}) and latent heat (LE_{EC}) fluxes, for the sake of more knowledge of glacio-meteorological characteristics. In Fig. 1a, a marked decline in the albedo mirrors the surface melt; α can exceed 0.6 over fresh snow, while its value is roughly fixed at 0.2 over melting bare ice (see also Weber 2007). Diurnal variations in $\overline{\theta}_0$ are well damped since late June, as expected over a melting ice surface. In Fig. 1b, the sign reversal of LE_{EC} values, i.e. from positive to negative, is identified in late June; it occurs with an increase in the relative humidity of ambient air that typically exceeds 70% when $LE_{EC} < 0$ becomes typical (figure omitted). The evolution in LE_{EC} indicates two phenomena: snow sublimation ($LE_{EC} > 0$) commonly takes place, and deposition/condensation ($LE_{EC} < 0$) is characteristic of the moisture exchange over melting valley glaciers (see also Oerlemans 2000; Andreassen et al. 2008; Giesen et al. 2008, 2009; van den Broeke et al. 2009). In mid-August, LE_{EC} shifts back to positive values (relative humidity typically below 70%), probably implying enhanced evaporation from meltwater streams and, to a lesser extent, effects of sporadic events of snowfall.

The above inspections of the evolution in albedo and latent heat flux make three melt phases distinguished, namely P1, P2, and P3 (see Fig. 1; 'P': period). P1, i.e. May 20–June 23, caters for a snow-covered surface. Snow depth (D) was initially measured to be about 0.5 m on May 20 and is assumed to be zero on June 23 in our study; its temporal variation, however, is not known precisely and described by empirical snowmelt equations (e.g. Singh and Singh 2001). We crudely make a linear interpolation of D on a daily basis to correct the reference heights: $z_M - D$ and $z_{T,q} - D$ in P1. These adjustments are found to have minor effects on the roughness length retrievals of z_{0M} and $z_{0T,q}$, which should not alter our conclusions. In P2, Bowen ratio ($\beta_{EC} = H_{EC}/LE_{EC}$) values are mostly positive—both H_{EC} and LE_{EC} represent an energy gain to the glacier. Their total contribution ($H_{EC} + LE_{EC}$) approaches 25% of the net energy budget (with the remaining 75% due to net radiation). β_{EC} has a median value of 3.4, which denotes a higher contribution by sensible heat fluxes over bare ice in P2 (see Fig. 1b).

4 Results

4.1 Examining Bowen-Ratio Similarity for Data Quality Check

The inequality $z_{0M} > z_{0T,q}$ is theoretically expected for aerodynamically rough flow. In our study, the roughness length retrievals that meet this expectation are called 'well-behaved' ($N = 348$); the rest are called 'unexpected' ($N = 139$), which account for nearly 30% out of a total of 487 half-hourly measurements.

The accuracy of roughness length retrievals of z_{0M} and $z_{0T,q}$ depends on both eddy-covariance fluxes and gradient measurements (see Sect. 2.1). To check the data quality, we consult 'Bowen-ratio similarity' that assumes downgradient transport of scalars with a common diffusion coefficient (cf. Foken 2008), or $\Psi_q = \Psi_T$ as assumed in Eq. 5. The Bowen ratio is then approximated using gradient data:

$$\beta_G = \gamma \frac{\Delta\overline{\theta}}{\Delta\overline{e}} = \frac{c_p P}{\varepsilon_m \lambda} \frac{\Delta\overline{\theta}}{\Delta\overline{e}}, \tag{12}$$

where the subscript G indicates this gradient-based estimate (β_G), γ is the psychrometric *constant*, P is the atmospheric pressure, $\varepsilon_m = 0.622$, i.e. the ratio of the molecular mass of water vapour to dry air, $\Delta\overline{e}$ denotes the surface-air difference in vapour pressure (e), namely $\Delta\overline{e} = \overline{e}_0 - \overline{e}_A$, where the subscripts '0' and 'A' represent the surface and the air, respectively. Ideally, β_G should match its counterpart derived from eddy-covariance measurements of turbulent heat fluxes, i.e. $\beta_{EC} = H_{EC}/LE_{EC}$. Figure 2 examines Bowen-ratio similarity by comparing β_G with β_{EC}.

In Fig. 2, Bowen-ratio similarity is reasonably supported by the data with 'well-behaved' roughness length retrievals (i.e. $z_{0M} > z_{0T,q}$), but clearly violated by those in the 'unexpected' category (i.e. $z_{0M} < z_{0T,q}$), which exhibit a significant scatter. Deviations appear most likely to occur at relatively high Bowen ratio with absolute values above one or so. This should be explicable by recognising the fact that high Bowen ratios (absolute values) are basically linked to a comparatively low amount of moisture exchange that, from a bulk-transfer perspective, partially results from diminished surface-air moisture difference. For confirmation, we investigate whether these two categories really differ in the magnitude of $\Delta\overline{\theta}$ or $\Delta\overline{e}$ measurements, which are used in β_G calculations (see Eq. 12). Minor differences in $\Delta\overline{\theta}$ are found between the two categories; $\Delta\overline{\theta}$ has an overall average of -4.8 ± 1.0 and -5.0 ± 0.8 K for the 'well-behaved' and 'unexpected' categories, respectively. Nonetheless, stark contrast in $\Delta\overline{e}$ exists: on average, its magnitude (i.e. $|\Delta\overline{e}|$) is markedly higher for the 'well-behaved' category, namely 85.3 ± 55.8 Pa compared to 25.8 ± 21.1 Pa for the other. Consequently, measurements of $\Delta\overline{e}$ are increasingly error-prone when $\Delta\overline{e}$ assumes a small magnitude, thus leading to significant errors in z_{0q} retrievals. Therefore, Fig. 2 is helpful to confirm that potential measurement errors are one primary cause of roughness length retrievals that violate the theoretically 'expected' relation $z_{0M} > z_{0T,q}$. Bowen-ratio similarity is validated by the data that produce 'well-behaved' retrievals that meet $z_{0M} > z_{0T,q}$, thereby lending support to the overall quality of our dataset. For continued analyses, we select a total of 323 half-hourly measurements, which simultaneously meet two constraints: $z_{0M} > z_{0T,q}$ (retrieved values) and $|\Delta\overline{e}| > 30$ Pa; this threshold value of $\Delta\overline{e}$ is adopted in order to reduce the use of data that are likely to suffer from significant measurement errors.

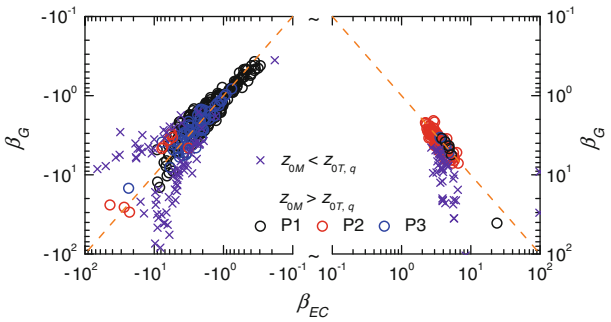

Fig. 2 Examining 'Bowen-ratio similarity' by a scatter plot of Bowen ratio estimations using gradient data (β_G) versus using eddy-covariance heat fluxes (β_{EC}). Based on z_{0M} and $z_{0T,q}$ retrievals, data points fall into two categories: 'unexpected' (*purple crosses*; $N = 139$) and 'well-behaved' (*open circles*; $N = 348$; further distinguished in colour among the three melt phases; see text for details)

4.2 Temporal Evolution and Diurnal Behaviour of the Roughness Lengths

To investigate how the roughness lengths evolve during this ablation season, Fig. 3 gives time series of the retrieved z_{0M}. In Fig. 3, z_{0M} exhibits a clear evolution, whose values nearly span three orders of magnitude (i.e. 10^{-4}–10^{-2} m). Given the snowfall on May 19, the first few data points (on May 20) seem to represent a fresh snow surface, where z_{0M} normally varies between 1.0×10^{-5} and 3.5×10^{-4} m (cf. Manes et al. 2008). In P1, the snowmelt process sees increasing z_{0M} values, typically on the order of 10^{-3} m (e.g. Bintanja 1995; Denby and Snellen 2002; Clifton et al. 2008; DeWalle and Rango 2008). At the P1–P2 transition, z_{0M} reaches a plateau and fluctuates around 10^{-2} m, possibly due to enhanced effects of the differential snowmelt. Afterwards, z_{0M} values decrease below 10^{-2} m over bare ice in P2 (e.g. Smeets et al. 1999). Over the Greenland ice sheet, Smeets and van den Broeke (2008a) found z_{0M} shifted in the opposite direction—it notably increased after snowmelt due to the exposed ice hummocks. This phenomenological difference leads us to infer that the initially snow-covered ice surface is not quite bumpy at the onset of the valley glacier seasonal melt. Once the ice is exposed, its differential melt gradually gives rise to meltwater streams and ice hummocks, whose growth ultimately results in high z_{0M} values above 10^{-2} m in P3 (see also Smeets et al. 1999; Brock et al. 2006).

The z_{0M} evolution in Fig. 3 indicates the changing topographic roughness during the ablation season. We are concerned that the growing roughness elements, ice hummocks in particular, could probably lead to a roughness sublayer. If this develops, the local airflow is undesirably subject to additional disturbance that undermines the rationale behind using the bulk aerodynamic method, such as Monin–Obukhov similarity theory. To detect the roughness sublayer's possible development, we check scalar turbulence characteristics, depicted by: (i) integral time scales (Λ_s), calculated with Eulerian autocorrelation functions, and (ii) vertical transport efficiency, quantified by linear correlation coefficients (R_{ws}) (see Stull 1988 and Roth and Oke 1995 for algorithms of Λ_s and R_{ws}, respectively; the subscript s represents a specific scalar). We hypothesise that, if a roughness sublayer develops (most likely in P3 over hummocky terrain), it should have a signature in the selected turbulence characteristics by inducing pronounced changes in Λ_s or R_{ws}. Figure 4a and b illustrate the time series of Λ_s and R_{ws}, respectively, where the subscript s is replaced by 'T' for temperature and 'q' for humidity.

In Fig. 4a, Λ_T and Λ_q represent characteristic time scales of turbulent eddies that transport temperature (T) and humidity (q), respectively. Most Λ_T values lie between 30 and 100 s, without discernible changes with time. Besides, Λ_q seems comparatively high in P2, when Bowen ratios (β) are typical positive; P1 and P3, both characterised by negative β, differ little in Λ_q, though P3 has a more hummocky surface. In Fig. 4b, R_{wT} and R_{wq} denote vertical

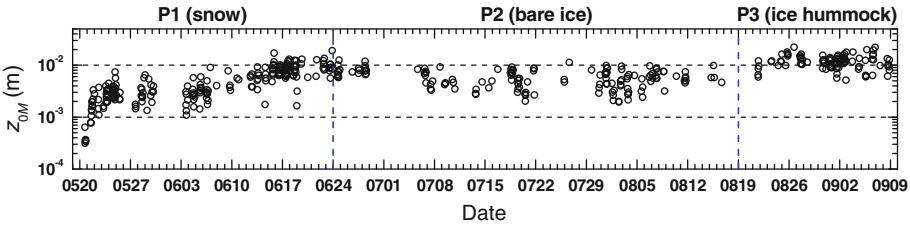

Fig. 3 Time series of the retrieved aerodynamic roughness length (z_{0M}). The *blue dashed lines* separate the three melt phases (P1, P2, and P3)

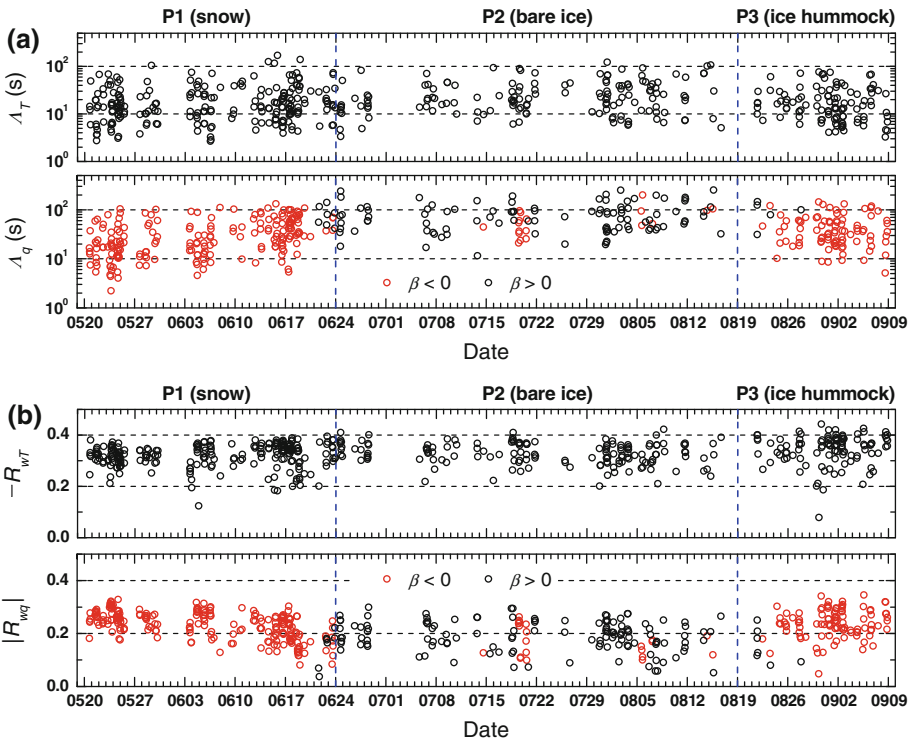

Fig. 4 Temporal evolution in scalar turbulence characteristics depicted by **a** integral time scales of temperature (Λ_T) and humidity (Λ_q), and **b** vertical transport efficiency of sensible heat (R_{wT}) and latent heat (R_{wq}). For depictions of Λ_q and R_{wq}, data points distinguish between negative (*red circles*) and positive (*black circles*) Bowen ratios (β). The *blue dashed lines* separate the three melt phases (P1, P2, and P3)

transport efficiencies of sensible heat and latent heat, respectively ($R_{ws} = \pm 1$ defines optimally efficient transport). R_{wT} hardly sees significant changes, with an overall average of -0.33 ± 0.05, a value close to those previously reported, such as -0.35 over a melting valley glacier (Weber 2007) and -0.38 in the interior of the Antarctic plateau (Basu et al. 2010). In general, R_{wq} (absolute values) has a clear evolution that suggests that the latent heat is more efficiently transported to the air through sublimation/evaporation ($\beta < 0$; P1 and P3) than to the surface through deposition/condensation ($\beta > 0$; P2). Somehow, we can discount the idea that a roughness sublayer develops during this ablation season.

Compared with z_{0M}, individual retrievals of z_{0T} and z_{0q} appear very scattered, which span more orders of magnitude (i.e. 10^{-6}–10^{-3} m for z_{0T} and 10^{-7}–10^{-2} m for z_{0q}) and hardly exhibit a discernible evolution by visual inspection (figure omitted). Instead, we wonder whether z_{0T} and z_{0q} behave differently in the diurnal cycle. Separately for each melt phase, Fig. 5 illustrates composite diurnal behaviours in z_{0M}, κB^{-1}, and κA^{-1} (retrieved values), as well as eddy-covariance measurements of the friction velocity (u_{*EC}) and turbulent heat fluxes (H_{EC} and LE_{EC}).

In Fig. 5, u_{*EC}, H_{EC}, and LE_{EC} have clear diurnal variations, which indicate that the turbulent exchange of momentum and energy peaks around 1600 LT with maximum katabatic wind speeds (correlated with high values of u_{*EC} as a surrogate; see Fig. 5a). As expected, from the knowledge that z_{0M} is mainly linked to the surface morphology rather than airflow

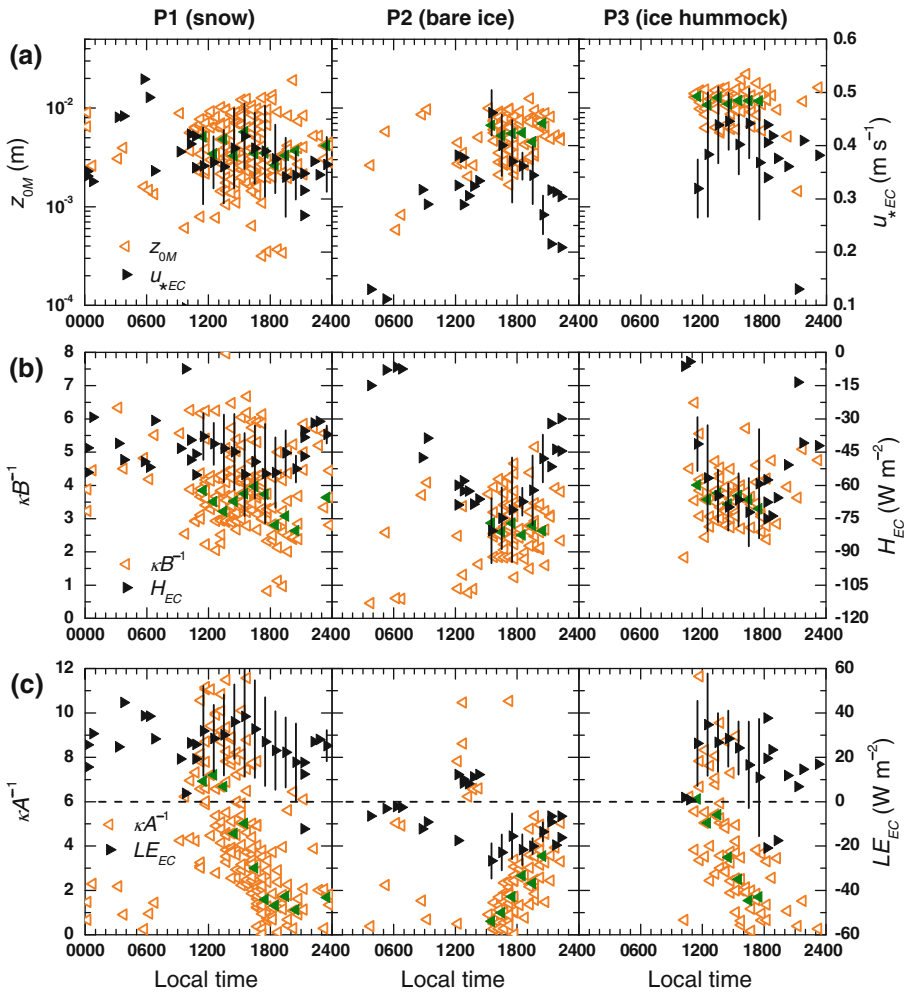

Fig. 5 Composite diurnal behaviours of **a** z_{0M} and u_{*EC}, **b** κB^{-1} and H_{EC}, and **c** κA^{-1} and LE_{EC}. *Left*, *middle*, and *right columns* correspond to the three melt phases P1, P2, and P3, respectively. For hourly bins with at least five data points, mean values and standard deviations (*error bars*) of u_{*EC}, H_{EC}, and LE_{EC} are illustrated to omit individual data points; *filled green triangles* denote hourly median values of z_{0M}, κB^{-1}, and κA^{-1} to ease visual inspection of their variability

properties, z_{0M} hardly exhibits a diurnal variation in Fig. 5a. A scatter plot of z_{0M} versus u_{*EC} confirms their negligible correlation (figure omitted). Thus, their 'fictitious correlation' arising from the use of Eq. 6 to retrieve z_{0M} is of less concern herein (see Andreas et al. 2005b for an in-depth examination).

In Fig. 5b, κB^{-1} values mostly lie between 0 and 8. This wide range of values makes it inappropriate to assume κB^{-1} (or z_{0M}/z_{0T}) as a constant value in glaciated areas, albeit an empirical approach adopted at times (cf. Garratt 1992; Bintanja 1995). Field studies over common land surfaces have found κB^{-1} highly variable and site-specific, with values widely spanning 0 to 20 over bare soil, grass, and shrub plant communities, where κB^{-1} exhibits a clear diurnal variation with peak values around noon (e.g. Verhoef et al. 1997;

Sun 1999; Su et al. 2001; Ma et al. 2008). Despite the lack of physical explanations, the κB^{-1} diurnal behaviour is normally linked to significant daily cycles of meteorological elements or turbulent parameters (e.g. Verhoef et al. 1997; Yang et al. 2003, 2008). In contrast, κB^{-1} does not exhibit a clear diurnal cycle over this valley glacier (see Fig. 5b). The melting ice/snow surface should be a main contributor, whose temperatures fluctuate around 273 K typically within a narrow interval (see $\overline{\theta}_0$ in Fig. 1a) and thus make $\Delta\overline{\theta}$ ($= \overline{\theta}_0 - \overline{\theta}_A$) cover a very limited diurnal range, i.e. merely 2 K or so.

Of interest in Fig. 5c is the observation that κA^{-1} exhibits evident diurnal variations. From about 1200 to 2000 LT, κA^{-1} is seemingly either decreasing or increasing with time, depending on the direction of moisture exchange (or, the sign of the Bowen ratio, β): in P1 and P3 ($LE_{EC} > 0$, sublimation/evaporation; $\beta < 0$), κA^{-1} decreases with time; in P2 ($LE_{EC} < 0$, deposition/condensation; $\beta > 0$), κA^{-1} increases with time. These variations in κA^{-1} appear to be monotonic overall and, therefore, their temporal phase mismatches that of LE_{EC} and u_{*EC}, both peaking around 1600 LT. By analogy with the $\Delta\overline{\theta}$ link to κB^{-1}, we consult the diurnal cycle of $\Delta\overline{q}$ ($= \overline{q}_0 - \overline{q}_A$) to help clarify the κA^{-1} behaviour. It turns out that $\Delta\overline{q}$ varies well in phase with κA^{-1} (figure omitted): for the period 1200–2000 LT, a decrease and increase in $|\Delta\overline{q}|$ are seen to accompany the processes of sublimation/evaporation ($\Delta\overline{q} > 0$ in P1 and P3) and deposition/condensation ($\Delta\overline{q} < 0$ in P2), respectively. Since the saturated surface has the $\overline{q}_0$ value vary little in a daily cycle, variations in $|\Delta\overline{q}|$ suggest that sublimation/evaporation and deposition/condensation processes see 'moistening' (increasing $\overline{q}_A$) and 'drying' (decreasing $\overline{q}_A$) in the katabatic wind regime, respectively, plausibly in line with the detailed moisture budget analysis in van den Broeke (1997a). So, $\Delta\overline{q}$ or related turbulent parameters (e.g. the scaling parameter of humidity, q_*) may be useful to help improve the z_{0q} or κA^{-1} parametrization in future studies.

4.3 Evaluating z_{0T} Parametrizations and the Sensible Heat-Flux Estimation

This section evaluates the z_{0T} parametrizations and uncovers their errors in estimating sensible heat fluxes. Colour-mapped by the roughness Reynolds number (Re_*), Fig. 6 is a scatter plot of z_{0T} versus z_{0M} (retrieved values). For reference, two envelopes of the $z_{0T} - z_{0M}$ dependence are also illustrated using the SvdB (upper, U) and A87 (lower, L) approaches, where u_* spans 0.1–0.6 m s^{-1} to cover the full range of our eddy-covariance measurements (see Fig. 5a).

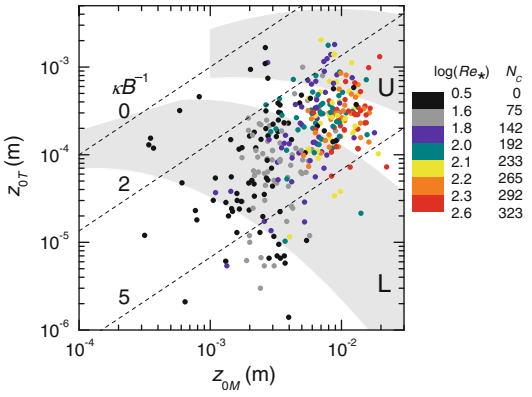

Fig. 6 Scatter plot of the retrieved z_{0T} versus z_{0M}, colour-mapped by Re_*. The *upper* (U) and *lower* (L) *grey areas* indicate the envelope of $z_{0T} - z_{0M}$ dependence modelled using parametrizations of Smeets and van den Broeke (2008b) and Andreas (1987), respectively ($0.1\,\text{m s}^{-1} < u_* < 0.6\,\text{m s}^{-1}$). *Dashed lines* are contours of κB^{-1}. N_c denotes the cumulative number of data points with increasing Re_*

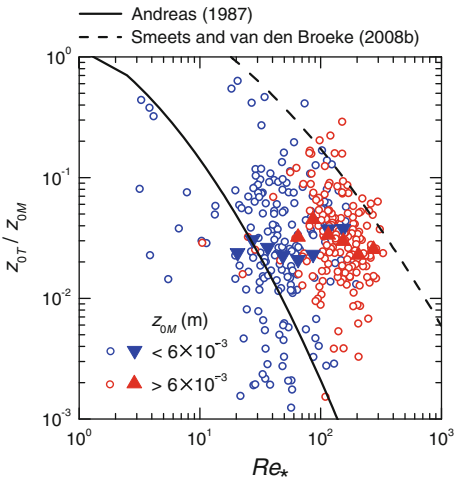

Fig. 7 Scatter plot of the ratio of z_{0T}/z_{0M} versus Re_*. Data points distinguish in colour between low ($< 6 \times 10^{-3}$ m, $N = 174$) and high ($> 6 \times 10^{-3}$ m, $N = 149$) z_{0M} values; in each category, *triangles* denote geometric mean values of z_{0T}/z_{0M} over Re_* bins of fixed width on the logarithmic scale (omitted when data points are too scarce). The parametrizations of Andreas (1987) and Smeets and van den Broeke (2008b) are shown for reference

In Fig. 6, the top and bottom border lines of each envelope correspond to u_* values of 0.1 and 0.6 m s^{-1}, respectively. For specific u_* and z_{0M}, SvdB (U) gives notably higher z_{0T} than A87 (L); moreover, with the increasing z_{0M}, z_{0T} modelled by the SvdB approach decreases much more slowly than that by A87. An interesting observation is that most data points with relatively low z_{0M} values straddle A87 (L), but those with higher z_{0M} frequently leave it to approach SvdB (U). A qualitative interpretation can be made for this behaviour. The colour-mapping in Fig. 6 shows a close correlation between z_{0M} and Re_* ($\equiv u_* z_{0M}/\nu$), as expected from the fact that u_* barely changes with the evolving z_{0M} (see Figs. 3, 5a). The data in various $\log(Re_*)$ intervals (see colour scale in Fig. 6) should thus have u_* values of similar magnitude overall. For specific u_*, the A87 approach models z_{0T} as a decreasing function of z_{0M}, in contrast to the opposite variability seen in the entire cloud of data points, hence their departure from A87 (L) at relatively high z_{0M} values.

Figure 6 makes us recall the novel finding in Smeets and van den Broeke (2008b): z_{0T} is underestimated by the A87 approach over high-z_{0M} rough ice, defined above an empirical z_{0M} threshold value of about 10^{-3} m (probably not universal but dependent on microscale roughness). Smeets and van den Broeke (2008b) associate the z_{0M} threshold value with the development of a roughness sublayer, where scalars are more efficiently 'ventilated'. Although the roughness sublayer development is deemed irrelevant herein, we wonder whether the present dataset also involves a z_{0M} threshold value. Following the Smeets and van den Broeke (2008b) definition, the data with z_{0M} below the threshold value should support Andreas's (1987) parametrization, while those with higher z_{0M} necessitate new coefficients in Eq. 8. In Fig. 6, we visually identify the threshold value as 6×10^{-3} m, which largely separates the data cloud into two clusters: one straddling A87 (L) and the other lying amidst A87 (L) and SvdB (U). Then, we need to determine whether the prescribed threshold value of 6×10^{-3} m is a meaningful counterpart of 10^{-3} m established in Smeets and van den Broeke (2008b).

Figure 7 plots the ratio of z_{0T}/z_{0M} (retrieved values) against the roughness Reynolds number (Re_*), where data points are differentiated using the z_{0M} threshold value of 6×10^{-3} m. To help detect the variation of z_{0T}/z_{0M} with Re_* in each category, geometric mean values[3] of z_{0T}/z_{0M} over equally sized Re_* bins on the logarithmic scale are shown by triangles.

[3] Geometric mean value is simply the exponential of the bin-average value of a variable's logarithm.

In Fig. 7, most data points lie between the curves of the A87 and SvdB approaches. Given the fact that z_{0M} values typically exceed 10^{-3} m in this dataset (see Fig. 3), Fig. 7 seems to support the finding in Smeets and van den Broeke (2008b): the A87 approach leads to underestimated z_{0T} when z_{0M} is higher than 10^{-3} m. Moreover, as the bin-averaged values indicate, the data points with $z_{0M} < 6 \times 10^{-3}$ m produce a z_{0T}/z_{0M} to Re_* relation clearly different from the Andreas (1987) curve, though the rest with $z_{0M} > 6 \times 10^{-3}$ m give a variability apparently similar to both curves. Therefore, the z_{0M} threshold value of 6×10^{-3} m is not an effective counterpart of 10^{-3} m found in Smeets and van den Broeke (2008b). The data cloud in Fig. 7 should then be largely regarded as an entirety; its scatter, however, hinders a regression of the coefficients in Eq. 8.

In fact, Smeets and van den Broeke (2008b) recognised the z_{0M} threshold value of 10^{-3} m using several datasets over an ice sheet/cap in Greenland/Iceland. It is of interest to determine its general relevance to glaciated areas. Over valley or outlet glaciers, Andreas's (1987) model of z_{0T} has mixed performance in earlier evaluations that cover a wide range of z_{0M} (or Re_*) values. For instance, Munro (1989) found z_{0T} notably underestimated by the A87 approach over ice $\left(z_{0M} = 2.5 \times 10^{-3}\ \text{m}\right)$ and snow $\left(z_{0M} = 5.5 \times 10^{-3}\ \text{m}\right)$ surfaces at Peyto Glacier (Canada). A major uncertainty in Munro's work arose from the height adjustment of profile measurements, which was one possible cause of the unexpected outcome of $z_{0M} < z_{0T}$ in Munro (1989). Andreas (2002) re-analysed Munro's dataset and found general support for Andreas's (1987) model for aerodynamically transitional flow (Re_* seldom exceeded 10, corresponding with $z_{0M} \sim 10^{-4}$ m). Denby and Snellen (2002) also found Andreas's (1987) model satisfactory over a melting outlet glacier in Iceland, where $10^{-4} < z_{0M} < 2 \times 10^{-3}$ m. Smeets and van den Broeke (2008b) validated Andreas's (1987) model using a dataset at Pasterze glacier (Austria) with $z_{0M} \approx 10^{-3}$ m (cf. Smeets et al. 1998). Combined with our results in Fig. 7, all these efforts suggest that Andreas's (1987) model works well at relatively low z_{0M}, i.e. roughly $10^{-4} < z_{0M} < 10^{-3}$ m; it is less reliable over surfaces with $z_{0M} > 10^{-3}$ m or so. Thus, we are led to tentatively argue that the z_{0M} threshold value remains relevant to valley or outlet glaciers, whose magnitude is about 10^{-3} m as empirically determined in Smeets and van den Broeke (2008b). Furthermore, judged from scalar turbulence characteristics (Fig. 4), our dataset suggests that a roughness sublayer does not necessarily develop even if z_{0M} exceeds its threshold value.

Figure 8 compares the estimated sensible heat fluxes (H_{BA}) with eddy-covariance measurements (H_{EC}); linear regressions of H_{BA} versus H_{EC} are made for overall evaluations. Table 2 gives comparative statistics for each melt phase and the whole ablation season, including the mean absolute difference (*MAD*), the mean bias estimate (*MBE*), the root-mean-square error (*RMSE*), and the mean absolute percentage difference (*MAPD*). Given the negative sign of H_{BA} and H_{EC}, a positive/negative *MBE* value indicates largely underestimated/overestimated sensible heat exchange.

In Fig. 8a and c, the sensible heat exchange is notably underestimated and overestimated by the A87 and SvdB approaches, respectively. *MBE* values in Table 2 signal some consistency with respect to their respective performance—A87 and SvdB consistently lead to underestimated and overestimated sensible heat exchange throughout this ablation season. One explicit cause is the significant underestimation and overestimation in z_{0T} by using the A87 and SvdB approaches, respectively (see Fig. 7). Comparing the statistics for each melt phase (see Table 2), we find that the SvdB approach performs better than A87 in both P2 and P3, since the former gives basically lower bias (*MBE*), deviation (*MAD* and *RMSE*), and relative difference (*MAPD*); and, A87 seemingly outperforms SvdB in P1 only. The SvdB approach thus turns out to be a beneficial adjustment to Andreas's (1987) original model for estimating sensible heat fluxes over an ice surface (i.e. in P2 and P3). Moreover, A87 and

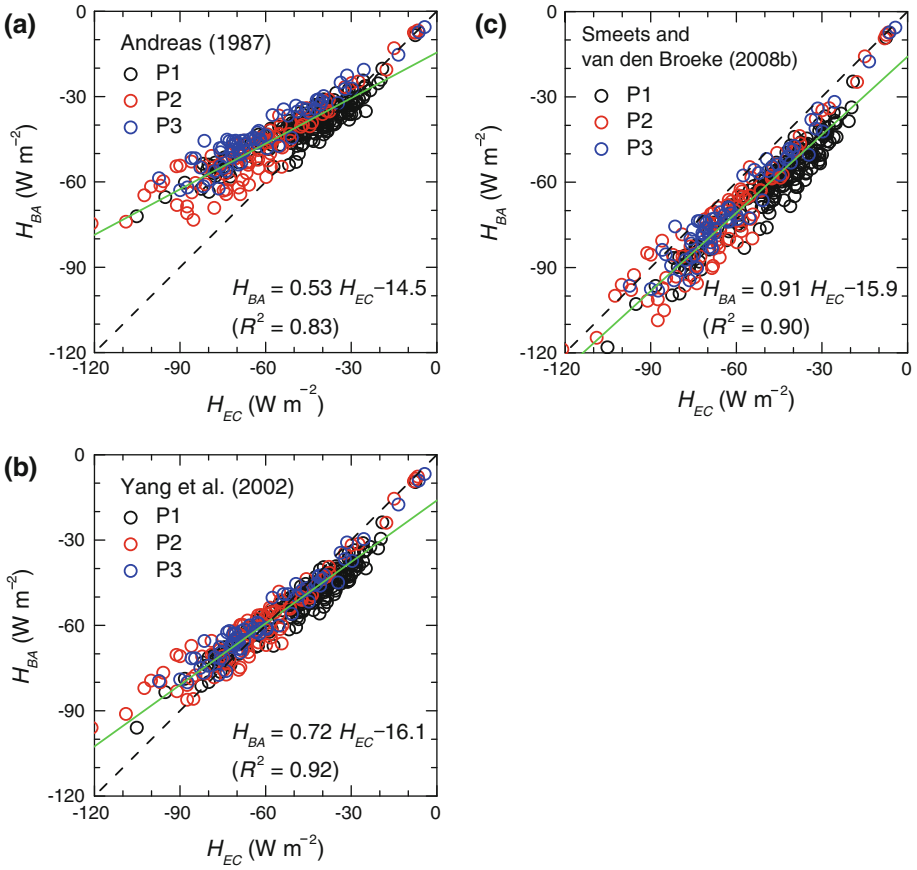

Fig. 8 Comparison in sensible heat fluxes between the bulk aerodynamic method (H_{BA}) and eddy-covariance method (H_{EC}). Data points distinguish among the three melt phases (P1, P2, and P3); least-squares linear regressions (*green line*) are made for an overall evaluation without distinguishing the data (regression equations given with coefficients of determination, i.e. R^2)

SvdB produce similar statistics for the whole ablation season, which generally underestimate and overestimate the sensible heat exchange nearly by 20%, respectively (see Table 2).

To our surprise, the sensible heat fluxes estimated by the Y02 approach appear fairly good in Fig. 8b. In Table 2, its optimal performance is confirmed by comparing the Y02 statistics with those of A87 and SvdB. Specifically, Y02's flux estimates lead to a much lower bias (*MBE*) and deviation (*MAD* and *RMSE*) than those of both A87 and SvdB; and, the Y02 approach gives relative differences (*MAPD*) that never exceed 15%. The linear regression in Fig. 8b, however, reveals Y02's deficiency owing to biased sensible heat-flux estimations—Y02 tends to underestimate high values of the sensible heat flux and overestimate low values. Specifically, sensible heat fluxes (absolute values) are typically higher over an ice surface (see P2 and P3 in Fig. 1b), which are generally underestimated by the Y02 approach, as indicated by positive *MBE* values in Table 2, and vice versa over a snow surface (P1) with a relatively low amount of sensible heat exchange (see Fig. 1b). For clarification, Fig. 9 compares the mean diurnal variations of κB^{-1} between three different z_{0T} parametrizations and the retrieval derived from quality-controlled data.

Table 2 Comparative statistics for sensible heat fluxes between the bulk aerodynamic method (H_{BA}) and eddy-covariance method (H_{EC}) using different parametrizations of z_{0T}

Period[a]	z_{0T} parametrization	*MAD* (W m^{-2})	*MBE* (W m^{-2})	*RMSE* (W m^{-2})	*MAPD* (%)
P1	Andreas (1987)	8.0	6.2	10.8	15
	Yang et al. (2002)	5.9	−4.1	7.0	15
	Smeets and van den Broeke (2008b)	13.8	−13.8	14.6	34
P2	Andreas (1987)	14.4	14.3	17.7	21
	Yang et al. (2002)	5.8	2.7	8.0	9
	Smeets and van den Broeke (2008b)	9.7	−9.0	11.5	17
P3	Andreas (1987)	17.6	17.4	19.5	28
	Yang et al. (2002)	4.9	2.5	6.2	10
	Smeets and van den Broeke (2008b)	7.8	−7.5	9.0	15
Overall	Andreas (1987)	11.6	10.5	14.8	19
	Yang et al. (2002)	5.8	−1.0	7.1	13
	Smeets and van den Broeke (2008b)	11.5	−11.3	10.9	20

[a] The results are presented separately for each melt phase (P1, P2, and P3) and the whole ablation season ('Overall')

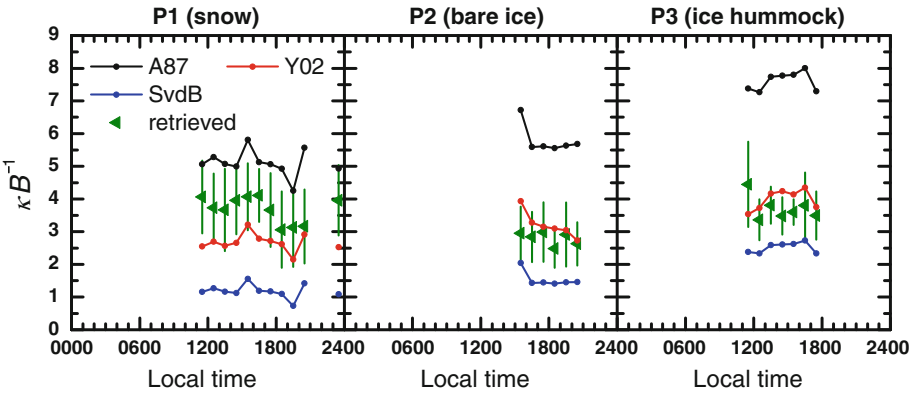

Fig. 9 Comparison in the mean diurnal variations of κB^{-1} between three different z_{0T} parametrizations and the retrieval derived from quality-controlled data. *Left*, *middle*, and *right columns* correspond to the three melt phases P1, P2, and P3, respectively. Illustrated are only for the hourly bins with at least five data points. The retrieved results (*green triangles*) are with *error bars* denoting standard deviations. Notice that the results using the Y02 and SvdB approaches also apply to κA^{-1}, due to the assumption $z_{0q} = z_{0T}$

In Fig. 9, the Y02 approach evidently differs from A87 and SvdB, which consistently overestimate and underestimate κB^{-1}, respectively; Y02's predictions appear much closer to the retrievals overall, thereby explaining its reliable sensible heat flux estimations (see Fig. 8b and Table 2). A closer look at κB^{-1} in individual melt phases reveals that the Y02 approach basically produces underestimates in P1, and slight overestimates in P2 and P3. Thus, Y02 leads to systematic errors in sensible heat-flux estimations during specific melt phases, i.e. overestimates in P1, and underestimates in P2 and P3. Based on Eq. 10, the Y02 approach makes z_{0T} vary with both u_* and $|H|$ in the opposite direction. Given the temporal evolution in H (Fig. 1b) and the largely uniform u_* during this ablation season (Fig. 5a),

the systematic errors in $|H|$ estimations should be mainly associated with the evolving magnitude of H. Specifically, higher z_{0T} values may be modelled in P1 with relatively low $|H|$ over snow, which result in underestimated κB^{-1} and, accordingly, overestimated $|H|$, and vice versa in P2 and P3 with relatively high $|H|$ over an ice surface.

Although the parametrization of Yang et al. (2002) is previously validated exclusively in (semi-)arid regions (e.g. Yang et al. 2009; Chen et al. 2010), the present evaluations make Y02 emerge as an approach equally useful in glaciated areas. We find fairly low errors in sensible heat-flux estimations using the Y02 approach, whose relative differences from eddy-covariance measurements remain below 15% throughout the ablation season. Y02 clearly outperforms the A87 and SvdB approaches, which consistently underestimate and overestimate the sensible heat exchange, respectively. Nonetheless, the Y02 approach gives apparently biased flux estimates, which could make it difficult to pinpoint their errors in practical use, particularly given the fact that sensible heat fluxes have a highly variable magnitude among the different melt phases (see Fig. 1b).

4.4 Evaluating z_{0q} Parametrizations and the Latent Heat-Flux Estimation

This section evaluates the z_{0q} parametrizations and tests their accuracy in latent heat-flux estimations. Figure 10 plots the ratio of z_{0q}/z_{0M} (retrieved values) against the roughness Reynolds number (Re_*), where data points distinguish among the three melt phases, namely P1, P2, and P3. Geometric mean values of z_{0q}/z_{0M} over equally sized Re_* bins on the logarithmic scale are illustrated, in order to detect the variation of z_{0q}/z_{0M} with Re_* for individual melt phases.

In Fig. 10, the data points are very scattered and wildly straddling the curves for the A87 and SvdB approaches, thus making it more of a challenge to evaluate the z_{0q} parametrizations (cf. Andreas 2002). As the bin-averaged values indicate, the retrievals of z_{0q}/z_{0M} over a snow surface (in P1) are roughly close to the predictions of Andreas (1987); but, those over an ice surface (in P2 and P3) are too scattered to be supportive of either parametrization. Overall, the retrieved z_{0q} values are notably higher than Andreas's (1987) predictions, particularly evident in P2 and P3. Given the fact that z_{0M} values are always above 10^{-3} m with few exceptions in the present dataset (see Fig. 3), Fig. 10 may confirm Smeets and van den Broeke's

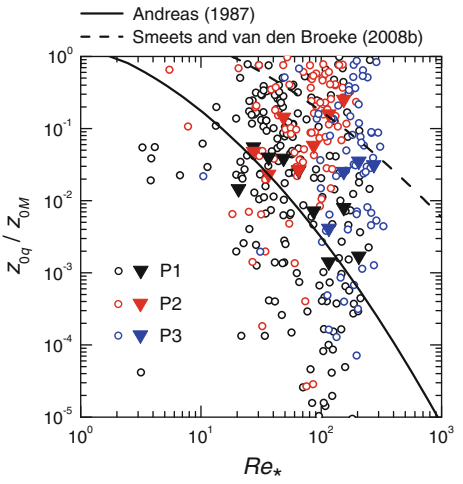

Fig. 10 Scatter plot of the ratio of z_{0q}/z_{0M} versus Re_*. Data points distinguish among the three melt phases (P1, P2, and P3). Separately for each melt phase, *triangles* denote geometric mean values of z_{0T}/z_{0M} over Re_* bins of fixed width on the logarithmic scale (omitted when data points are too scarce). The parametrizations of Andreas (1987) and Smeets and van den Broeke (2008b) are shown for reference

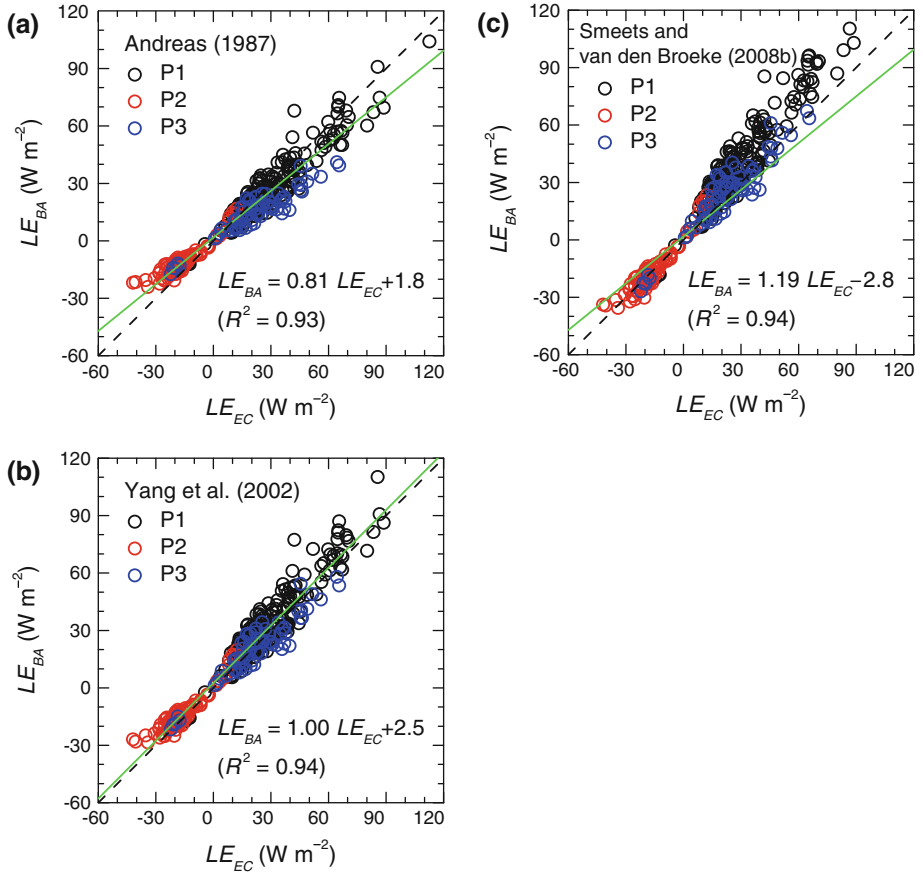

Fig. 11 Comparison in latent heat fluxes between the bulk aerodynamic method (LE_{BA}) and eddy-covariance method (LE_{EC}). Data points distinguish among the three melt phases (P1, P2, and P3); least-squares linear regressions (*green line*) are made for an overall evaluation without distinguishing the data (regression equations given with coefficients of determination, i.e. R^2)

(2008b) finding that the A87 approach leads to significant underestimates in z_{0q}, when z_{0M} exceeds the threshold value of 10^{-3} m or so. Nonetheless, the SvdB approach, proposed for use specifically over rough ice (i.e. $z_{0M} > 10^{-3}$ m), tends to overestimate z_{0q} values in all the melt phases (see Fig. 10). We proceed to evaluate the latent heat-flux estimations using the three candidate parametrizations of z_{0q}.

Figure 11 compares the estimated latent heat fluxes (LE_{BA}) with eddy-covariance measurements (LE_{EC}). Comparative statistics are available in Table 3, where *MAD*, *MBE*, *RMSE*, and *MAPD* are computed separately for each melt phase and the whole ablation season. Since the sign of the latent heat fluxes distinguishes between sublimation/evaporation (positive) and deposition/condensation (negative), the *MBE* value has opposite suggestive meaning when used to evaluate the two different types of moisture exchange. That is, a positive/negative *MBE* value indicates largely overestimated/underestimated amount of sublimation or evaporation (primarily in P1 and P3), and vice versa for the evaluation of deposition or condensation in P2 (see Fig. 1b). Such a mixed meaning, therefore, renders the *MBE* value less usable for flux evaluation over the whole ablation season. We have to consult the linear regressions between LE_{BA} and LE_{EC} instead (see Fig. 11).

Table 3 Comparative statistics for latent heat fluxes between the bulk aerodynamic method (LE_{BA}) and eddy-covariance method (LE_{EC}) using different parametrizations of z_{0q}

Period[a]	z_{0q} parametrization	*MAD* (W m^{-2})	*MBE* (W m^{-2})	*RMSE* (W m^{-2})	*MAPD* (%)
P1	Andreas (1987)	5.7	−2.4	7.1	20
	Yang et al. (2002)	6.7	4.2	8.5	25
	Smeets and van den Broeke (2008b)	11.3	10.7	14.4	39
P2	Andreas (1987)	6.6	6.6	7.7	31
	Yang et al. (2002)	3.8	3.1	4.8	17
	Smeets and van den Broeke (2008b)	2.8	−0.3	3.4	14
P3	Andreas (1987)	9.1	−7.8	11.4	32
	Yang et al. (2002)	5.6	−1.9	6.8	22
	Smeets and van den Broeke (2008b)	5.4	1.7	6.9	25
Overall	Andreas (1987)	6.6	−1.6	8.3	25
	Yang et al. (2002)	5.8	2.7	7.5	23
	Smeets and van den Broeke (2008b)	8.2	6.5	11.5	31

[a] The results are presented separately for each melt phase (P1, P2, and P3) and the whole ablation season ('Overall')

In Fig. 11a and c, the A87 and SvdB approaches generally underestimate and overestimate the latent heat fluxes (absolute values), respectively. *MBE* values in Table 3 suggest their uniform performance—A87 and SvdB consistently lead to an underestimated and overestimated amount of moisture exchange in individual melt phases, be it in the form of sublimation/evaporation (positive fluxes in P1 and P3) or deposition/condensation (negative fluxes in P2). One major contributor to this outcome is the notable underestimation and overestimation in z_{0q} by using the A87 and SvdB approaches, respectively (see Fig. 10). The statistics in Table 3 indicate that the SvdB approach outperforms A87 over an ice surface (i.e. in P2 and P3), as SvdB produces a much lower bias (*MBE*), deviation (*MAD* and *RMSE*), and relative difference (*MAPD*); and, A87 performs better than SvdB over a snow surface (in P1) only. Judged by these evaluations, we regard the SvdB approach a helpful adjustment to Andreas's (1987) original model for estimating latent heat fluxes over an ice surface (i.e. in P2 and P3).

Both the A87 and SvdB approaches, however, can lead to notable errors, as indicated by the *MAPD* values even exceeding 30% for specific melt phases. In comparison, the Y02 approach seems promising, due to its lower statistics in general (see Table 3). Also, Y02 produces the lowest errors over the whole ablation season, as represented by *MAD* (5.8 W m^{-2}), *RMSE* (7.1 W m^{-2}), and *MAPD* (13%) values. A comparison of the linear regressions in Fig. 11 lends further support to the Y02 approach. Given that their intercepts are rather close to zero, slope values can be roughly interpreted as an indicator of relative errors. Accordingly, the A87 and SvdB approaches give underestimated and overestimated moisture exchange nearly by 20% overall, respectively (see Fig. 11a, c). In contrast, latent heat fluxes estimated by the Y02 approach are more satisfactory, which compare to eddy-covariance measurements with a perfect slope of unity in Fig. 11b.

Recalling the sensible heat-flux evaluations in Sect. 4.3, we find some consistency in the performance of the candidate parametrizations—applying both to individual melt phases and to the whole ablation season—the A87 and SvdB approaches generally give underestimated and overestimated amounts for the heat exchange, respectively, viz. both sensible heat and latent heat fluxes; overall, the Y02 approach gives the most accurate estimations, though

Y02 tends to overestimate both sensible heat and latent heat fluxes over a snow surface (in P1) and underestimate them over an ice surface (in P2 and P3), as indicated by the sign of *MBE* values in Tables 2 and 3. All these findings should lead us to recommend the Y02 approach as a hopefully feasible one for the scalar roughness length parametrization in glaciated areas.

In fact, all the three candidate parametrizations have one common deficiency: none of them is able to produce the $\kappa \mathrm{A}^{-1}$ diurnal variations as retrieved in Fig. 5c, which clearly mismatch those modelled using the A87, Y02, and SvdB approaches (see Fig. 9 for reference). Such a mismatch in the diurnal cycle of $\kappa \mathrm{A}^{-1}$, therefore, leads to inevitable effects on the daily course of latent heat-flux estimations using the bulk aerodynamic method, thereby causing errors in the surface energy budget or mass balance modelling at a fine temporal resolution. Future efforts to develop or improve z_{0q} $\left(\text{or } \kappa A^{-1}\right)$ parametrizations should take the diurnal variations into account (see Fig. 5c), probably by incorporating new meteorological or turbulent parameters, such as $\Delta\overline{q}$ and q_*.

5 Concluding Remarks and Recommendation

We report on a short-term field campaign over a melting valley glacier on the Tibetan Plateau. In our study, quality-controlled measurements are used to critically evaluate three parametrizations of the scalar roughness lengths; they stem from Andreas (1987), Yang et al. (2002), and Smeets and van den Broeke (2008b), abbreviated as the A87, Y02, and SvdB approaches, respectively. Specific findings and recommendations include:

(i) During this ablation season, the aerodynamic roughness length (z_{0M}) varies on the order of 10^{-4}–10^{-2} m, whose evolution corresponds to three melt phases distinguished with surface cover and moisture exchange: snow (sublimation/evaporation), bare ice (deposition/condensation), and ice hummocks (sublimation/evaporation). Selected characteristics of scalar turbulence over smooth snow differ little from those over hummocky ice, thereby implying the absence of a roughness sublayer.

(ii) Bowen-ratio similarity is validated in the katabatic flow, which has useful implications for glacio-meteorological investigations. First, Bowen-ratio similarity is helpful for checking the data quality of both turbulent fluxes and vertical temperature/humidity gradients. This argument is based on the finding that Bowen-ratio similarity is well supported by the data that give roughness length retrievals meeting the expected relation $z_{0M} > z_{0T,q}$; and, it is frequently violated by those undesirably leading to $z_{0M} < z_{0T,q}$. Second, the validity of Bowen-ratio similarity introduces a feasible means for flux measurements in glaciated areas. Specifically, with the Bowen ratio derived from gradient data (see Eq. 12), either sensible heat or latent heat fluxes can then be estimated only if measurements for a single type of turbulent heat exchange are available.

(iii) The excess resistances to scalar transfer of $\kappa \mathrm{B}^{-1}$ (for temperature) and $\kappa \mathrm{A}^{-1}$ (for humidity) behave differently in the diurnal cycle. $\kappa \mathrm{B}^{-1}$ does not exhibit an evident diurnal variation, possibly due to the very narrow diurnal range of surface-air temperature difference ($\Delta\overline{\theta}$) over a melting surface (i.e. 2 K or so). In contrast, $\kappa \mathrm{A}^{-1}$ clearly decreases and increases with time in conditions of sublimation/evaporation and deposition/condensation, respectively. Its evolution is accompanied by the 'moistening' ('drying') in the katabatic flow with the occurrence of sublimation/evaporation (deposition/condensation).

(iv) The A87 and SvdB approaches generally lead to underestimated and overestimated amounts of both types of turbulent heat exchange, respectively—consistently found among the individual melt phases and over the whole ablation season. An explicit cause is the notable underestimation and overestimation in $z_{0T,q}$ values by using A87 and SvdB, respectively. We find SvdB a beneficial adjustment to Andreas's (1987) original model over a rough ice surface (i.e. in P2 and P3 herein), which is empirically defined as $z_{0M} > 10^{-3}$ m by Smeets and van den Broeke (2008b). This z_{0M} threshold value is considered of general relevance to glaciated areas (e.g. ice sheet/cap and valley/outlet glaciers), irrespective of the development of the roughness sublayer. Compared with significant errors in the heat-flux estimations using A87 and SvdB, much lower errors are produced by the Y02 approach, which, previously validated in (semi-)arid regions only, turns out equally useful to parametrize $z_{0T,q}$ in glaciated areas. Although Y02 deserves a recommendation for practical use, biased sensible heat-flux estimates are observed—the Y02 approach underestimates (overestimates) relatively high (low) values of sensible heat flux. Interestingly, this outcome sees a link to the surface cover, given the fact that the underestimates and overestimates basically occur over an ice surface (in P2 and P3) and a snow surface (in P1), respectively. We thus encourage continued evaluations using high-quality field measurements in glaciated areas, particularly for future improvements. Meanwhile, we call attention to one deficiency of all the three candidate parametrizations, i.e. the failure to produce diurnal variations in κA^{-1} as retrieved in Fig. 5c. New meteorological or turbulent parameters (e.g. $\Delta\overline{q}$ and q_*) may probably help with an improved z_{0q} parametrization.

Acknowledgements The single anonymous reviewer has the authors' heartfelt gratitude, whose critical comments have led us to improve our data analysis and writing. During our fieldwork preparation, we were lucky to receive thoughtful consultation from Xuelong Chen, Shichang Kang, Jingshi Liu, Xin Liu, Yaoming Ma, Jun Qin, Lide Tian, Yongjie Wang, and Baiqing Xu. Drs. Günther Heinemann (University of Trier) and Johannes Oerlemans (Utrecht University) provided several up-to-date references helpful to our knowledge of glacio-meteorology. This study is jointly funded by the Chinese Academy of Sciences (CAS Innovation Project KZCX2-YW-145), China Postdoctoral Science Foundation (Grant 20090450056), and National Natural Science Foundation of China (Grant 40905003 and 40901047). Xiaofeng Guo gratefully acknowledges the support of K. C. Wong Education Foundation, Hong Kong. The Southeast Tibet Observation and Research Station for the Alpine Environment (SETORS, CAS) provided logistic support that greatly facilitated our fieldwork.

References

Anderson PS, Neff WD (2008) Boundary layer physics over snow and ice. Atmos Chem Phys 8:3563–3582

Andreas EL (1987) A theory for the scalar roughness and the scalar transfer coefficients over snow and sea ice. Boundary-Layer Meteorol 38:159–184

Andreas EL (2002) Parameterizing scalar transfer over snow and ice: a review. J Hydrometeorol 3:417–432

Andreas EL, Persson POG, Jordan RE, Horst TW, Guest PS, Grachev AA, Fairall CW (2004) Roughness lengths over snow. In: Proceedings of 84th AMS annual meeting, paper JP4.31, Seattle, WA, USA, 8 pp

Andreas EL, Jordan RE, Makshtas AP (2005a) Parameterizing turbulent exchange over sea ice: the Ice Station Weddell results. Boundary-Layer Meteorol 114:439–460

Andreas EL, Persson POG, Jordan RE, Horst TW, Guest PS, Grachev AA, Fairall CW (2005b) Parameterizing the turbulent surface fluxes over summer sea ice. In: Proceedings of 85th AMS annual meeting, paper J1.15, San Diego, CA, USA, 9 pp

Andreas EL, Horst TW, Grachev AA, Persson POG, Fairall CW, Guest PS, Jordan RE (2010a) Parametrizing turbulent exchange over summer sea ice and the marginal ice zone. Q J Roy Meteorol Soc 136:927–943

Andreas EL, Persson POG, Jordan RE, Horst TW, Guest PS, Grachev AA, Fairall CW (2010b) Parameterizing turbulent exchange over sea ice in winter. J Hydrometeorol 11:87–104

Andreassen LM, van den Broeke MR, Giesen RH, Oerlemans J (2008) A 5 year record of surface energy and mass balance from the ablation zone of Storbreen, Norway. J Glaciol 54:245–258
Basu S, Ruiz-Columbié A, Phillipson JA, Harshan S (2010) Local scaling characteristics of Antarctic surface layer turbulence. Cryosphere 4:325–331
Bintanja R (1995) The local surface energy balance of the Ecology Glacier, King George Island, Antarctica: measurements and modelling. Antarct Sci 7:315–325
Bintanja R, van den Broeke MR (1995) Momentum and scalar transfer coefficients over aerodynamically smooth Antarctic surfaces. Boundary-Layer Meteorol 74:89–111
Brock BW, Willis IC, Sharp MJ (2006) Measurement and parameterization of aerodynamic roughness length variations at Haut Glacier d'Arolla, Switzerland. J Glaciol 52:281–297
Brunke MA, Zhou M, Zeng X, Andreas EL (2006) An intercomparison of bulk aerodynamic algorithms used over sea ice with data from the Surface Heat Budget for the Arctic Ocean (SHEBA) experiment. J Geophys Res 111:C09001. doi:10.1029/2005JC002907
Cassano JJ, Parish TR, King JC (2001) Evaluation of turbulent surface flux parameterizations for the stable surface layer over Halley, Antarctica. Mon Weather Rev 129:26–46
Chen Y, Yang K, Zhou D, Qin J, Guo X (2010) Improving Noah land surface model in arid regions with an appropriate parameterization of the thermal roughness length. J Hydrometeorol 11:995–1006
Chiba O, Kobayashi S (1986) A study of the structure of low-level katabatic winds at Mizuho Station, East Antarctica. Boundary-Layer Meteorol 37:343–355
Clifton A, Manes C, J-D Rüedi, Guala M, Lehning M (2008) On shear-driven ventilation of snow. Boundary-Layer Meteorol 126:249–261
Davidson PA (2004) Turbulence: an introduction for scientists and engineers. Oxford University Press, Oxford, 657 pp
Denby B, Greuell W (2000) The use of bulk and profile methods for determining surface heat fluxes in the presence of glacier winds. J Glaciol 46:445–452
Denby B, Snellen H (2002) A comparison of surface renewal theory with the observed roughness length for temperature on a melting glacier surface. Boundary-Layer Meteorol 103:459–468
DeWalle DR, Rango A (2008) Principles of snow hydrology. Cambridge University Press, Cambridge, 403 pp
Foken T (2008) Micrometeorology. Springer, Heidelberg, 308 pp
Foken T, Göckede M, Mauder M, Mahrt L, Amiro B, Munger W (2004) Post-field data quality control. In: Lee X, Massman W, Law B (eds) Handbook of micrometeorology: a guide for surface flux measurement and analysis. Kluwer, Dordrecht pp 181–208
Forrer J, Rotach MW (1997) On the turbulence structure in the stable boundary layer over the Greenland ice sheet. Boundary-Layer Meteorol 85:111–136
Garratt JR (1992) The atmospheric boundary layer. Cambridge University Press, Cambridge, 316 pp
Giesen RH, van den Broeke MR, Oerlemans J, Andreassen LM (2008) Surface energy balance in the ablation zone of Midtdalsbreen, a glacier in southern Norway: interannual variability and the effect of clouds. J Geophys Res 113:D21111. doi:10.1029/2008JD010390
Giesen RH, Andreassen LM, van den Broeke MR, Oerlemans J (2009) Comparison of the meteorology and surface energy balance at Storbreen and Midtdalsbreen, two glaciers in southern Norway. Cryosphere 3:57–74
Greuell W, Genthon C (2004) Modelling land-ice surface mass balance. In: Bamber JL, Payne AJ (eds) Mass balance of the cryosphere: observations and modelling of contemporary and future changes. Cambridge University Press, Cambridge pp 117–168
Haverd V, Böhm M, Raupach MR (2010) The effect of source distribution on bulk scalar transfer between a rough land surface and the atmosphere. Boundary-Layer Meteorol 135:351–368
Heinemann G (2004) Local similarity properties of the continuously turbulent stable boundary layer over Greenland. Boundary-Layer Meteorol 112:283–305
Heinemann G (2008) The polar regions: a natural laboratory for boundary layer meteorology—a review. Meteorol Z 17:589–601
Hock R (2005) Glacier melt: a review of processes and their modelling. Prog Phys Geogr 29:362–391
Holtslag AAM, de Bruin HAR (1988) Applied modeling of the nighttime surface energy balance over land. J Appl Meteorol 27:689–704
Hudson SR, Brandt RE (2005) A look at the surface-based temperature inversion on the Antarctic plateau. J Clim 18:1673–1696
Kaimal JC, Finnigan JJ (1994) Atmospheric boundary layer flows: their structure and measurement. Cambridge University Press, Cambridge, 289 pp
Kaimal JC, Wyngaard JC, Izumi Y, Coté OR (1972) Spectral characteristics of surface-layer turbulence. Q J Roy Meteorol Soc 98:563–589

King JC (1990) Some measurements of turbulence over an Antarctic ice shelf. Q J Roy Meteorol Soc 116:379–400
King JC, Argentini SA, Anderson PS (2006) Contrasts between the summertime surface energy balance and boundary layer structure at Dome C and Halley stations, Antarctica. J Geophys Res 111:D02105. doi:10.1029/2005JD006130
Klok EJ, Nolan M, van den Broeke MR (2005) Analysis of meteorological data and the surface energy balance of McCall Glacier, Alaska, USA. J Glaciol 51:451–461
Konya K, Matsumoto T (2010) Influence of weather conditions and spatial variability on glacier surface melt in Chilean Patagonia. Theor Appl Climatol 102:139–149
Lee X, Finnigan J, Paw U KT (2004) Coordinate systems and flux bias error. In: Lee X, Massman W, Law B (eds) Handbook of micrometeorology: a guide for surface flux measurement and analysis. Kluwer, Dordrecht pp 33–66
Liebethal C, Foken T (2003) On the significance of the Webb correction to fluxes. Boundary-Layer Meteorol 109:99–106
Liebethal C, Foken T (2004) On the significance of the Webb correction to fluxes: corrigendum. Boundary-Layer Meteorol 113:301
Ma Y, Menenti M, Feddes R, Wang J (2008) Analysis of the land surface heterogeneity and its impact on atmospheric variables and the aerodynamic and thermodynamic roughness lengths. J Geophys Res 113:D08113. doi:10.1029/2007JD009124
Mahrt L (2010) Computing turbulent fluxes near the surface: needed improvements. Agric For Meteorol 150:501–509
Manes C, Guala M, Löwe H, Bartlett S, Egli L, Lehning M (2008) Statistical properties of fresh snow roughness. Water Resour Res 44:W11407. doi:10.1029/2007WR006689
Mauder M, Foken T (2006) Impact of post-field data processing on eddy covariance flux estimates and energy balance closure. Meteorol Z 15:597–609
McMillen RT (1988) An eddy correlation technique with extended applicability to non-simple terrain. Boundary-Layer Meteorol 43:231–245
Meesters AGCA, Bink NJ, Vugts HF, Cannemeijer F, Henneken EAC (1997) Turbulence observations above a smooth melting surface on the Greenland ice sheet. Boundary-Layer Meteorol 85:81–110
Moore CJ (1986) Frequency response corrections for eddy correlation systems. Boundary-Layer Meteorol 37:17–35
Munro DS (1989) Surface roughness and bulk heat transfer on a glacier: comparison with eddy correlation. J Glaciol 35:343–348
Munro DS (2006) Linking the weather to glacier hydrology and mass balance at Peyto glacier. In: Demuth MN, Munro DS, Young GT (eds) Peyto glacier: one century of science. National Hydrology Research Institute Science Report, vol 8, pp 135–178
Munro DS, Davies JA (1977) An experimental study of the glacier boundary layer over melting ice. J Glaciol 18:425–436
Munro DS, Davies JA (1978) On fitting the log-linear model to wind speed and temperature profiles over a melting glacier. Boundary-Layer Meteorol 15:423–437
Oerlemans J (1998) The atmospheric boundary layer over melting glaciers. In: Holtslag AAM, Duynkerke PG (eds) Clear and cloudy boundary layers. Royal Netherlands Academy of Arts and Sciences, Amsterdam pp 129–153
Oerlemans J (2000) Analysis of a 3 year meteorological record from the ablation zone of Morteratschgletscher, Switzerland: energy and mass balance. J Glaciol 46:571–579
Oerlemans J (2001) Glaciers and climate change. A.A. Balkema Publishers, Rotterdam, 148 pp
Oerlemans J (2010) The microclimate of valley glaciers. Utrecht Publishing & Archiving Services (Utrecht University), Igitur, 138 pp
Oerlemans J, Grisogono B (2002) Glacier winds and parameterisation of the related surface heat fluxes. Tellus A 54:440–452
Oerlemans J, Klok EJ (2002) Energy balance of a glacier surface: analysis of automatic weather station data from the Morteratschgletscher, Switzerland. Arct Antarct Alp Res 34:477–485
Oerlemans J, Björnsson H, Kuhn M, Obleitner F, Palsson F, Smeets CJPP, Vugts HF, De Wolde J (1999) Glacio-meteorological investigations on Vatnajökull, Iceland, summer 1996: an overview. Boundary-Layer Meteorol 92:3–26
Parish TR, Cassano JJ (2003) The role of katabatic winds on the Antarctic surface wind regime. Mon Weather Rev 131:317–333
Parmhed O, Oerlemans J, Grisogono B (2004) Describing surface fluxes in katabatic flow on Breidamerkurjökull, Iceland. Q J Roy Meteorol Soc 130:1137–1151

Pasricha PK, Singh R, Sarkar SK, Dutta HN, Reddy BM, Das PK (1991) Characteristics of atmospheric turbulence in the surface layer over Antarctica. Boundary-Layer Meteorol 57:207–217
Roth M, Oke TR (1995) Relative efficiencies of turbulent transfer of heat, mass, and momentum over a patchy urban surface. J Atmos Sci 52:1863–1874
Schotanus P, Nieuwstadt FTM, De Bruin HAR (1983) Temperature measurement with a sonic anemometer and its application to heat and moisture fluctuations. Boundary-Layer Meteorol 26:81–93
Singh P, Singh VP (2001) Snow and glacier hydrology. Kluwer, Dordrecht, 742 pp
Smeets CJPP, Duynkerke PG, Vugts HF (1998) Turbulence characteristics of the stable boundary layer over a mid-latitude glacier. Part I: A combination of katabatic and large-scale forcing. Boundary-Layer Meteorol 87:117–145
Smeets CJPP, Duynkerke PG, Vugts HF (1999) Observed wind profiles and turbulence fluxes over an ice surface with changing surface roughness. Boundary-Layer Meteorol 92:101–123
Smeets CJPP, Duynkerke PG, Vugts HF (2000) Turbulence characteristics of the stable boundary layer over a mid-latitude glacier. Part II: Pure katabatic forcing conditions. Boundary-Layer Meteorol 97:73–107
Smeets CJPP, van den Broeke MR (2008a) Temporal and spatial variations of the aerodynamic roughness length in the ablation zone of the Greenland ice sheet. Boundary-Layer Meteorol 128:315–338
Smeets CJPP, van den Broeke MR (2008b) The parameterisation of scalar transfer over rough ice. Boundary-Layer Meteorol 128:339–355
Stössel F, Guala M, Fierz C, Manes C, Lehning M (2010) Micrometeorological and morphological observations of surface hoar dynamics on a mountain snow cover. Water Resour Res 46:W04511. doi:10.1029/2009WR008198
Stull R (1988) An introduction to boundary layer meteorology. Kluwer, Dordrecht, 297 pp
Su Z, Schmugge T, Kustas WP, Massman WJ (2001) An evaluation of two models for estimation of the roughness height for heat transfer between the land surface and the atmosphere. J Appl Meteorol 40:1933–1951
Sun J (1999) Diurnal variations of thermal roughness height over a grassland. Boundary-Layer Meteorol 92:407–427
Townsend AA (1976) The structure of turbulent shear flow. Cambridge University Press, Cambridge, 429 pp
Tsonis AA (2002) An introduction to atmospheric thermodynamics. Cambridge University Press, Cambridge, 182 pp
van den Broeke MR (1997a) Momentum, heat, and moisture budgets of the katabatic wind layer over a mid-latitude glacier in summer. J Appl Meteorol 36:763–774
van den Broeke MR (1997b) Structure and diurnal variation of the atmospheric boundary layer over a mid-latitude glacier in summer. Boundary-Layer Meteorol 83:183–205
van den Broeke M, Reijmer C, van As D, Boot W (2006) Daily cycle of the surface energy balance in Antarctica and the influence of clouds. Int J Climatol 26:1587–1605
van den Broeke M, Smeets P, Ettema J, van der Veen C, van de Wal R, Oerlemans J (2008) Partitioning of melt energy and meltwater fluxes in the ablation zone of the west Greenland ice sheet. Cryosphere 2:179–189
van den Broeke M, Smeets P, Ettema J (2009) Surface layer climate and turbulent exchange in the ablation zone of the west Greenland ice sheet. Int J Climatol 29:2309–2323
van der Avoird E, Duynkerke PG (1999) Turbulence in a katabatic flow: does it resemble turbulence in stable boundary layers over flat surfaces. Boundary-Layer Meteorol 92:39–66
Verhoef A, De Bruin HAR, van den Hurk BJJM (1997) Some practical notes on the parameter kB^{-1} for sparse vegetation. J Appl Meteorol 36:560–572
Vihma T, Launiainen J, Pirazzini R (2009) 20 Years of Finnish research on boundary-layer meteorology and air–ice–sea interaction in the Antarctic. Geophysica 45:7–26
Webb EK, Pearman GI, Leuning R (1980) Correction of flux measurements for density effects due to heat and water vapour transfer. Q J Roy Meteorol Soc 106:85–100
Weber M (2007) A parameterization for the turbulent fluxes over melting surfaces derived from eddy correlation measurements. In: Proceedings of Alpine-snow-workshop, Nationalpark Berchtesgaden, Munich, Germany, pp 138–149
Xu B-Q, Wang M, Joswiak DR, Cao J-J, Yao T-D, Wu G-J, Yang W, Zhao H-B (2009) Deposition of anthropogenic aerosols in a southeastern Tibetan glacier. J Geophys Res 114:D17209. doi:10.1029/2008JD011510
Yang K, Koike T, Fujii H, Tamagawa K, Hirose N (2002) Improvement of surface flux parameterizations with a turbulence-related length. Q J Roy Meteorol Soc 128:2073–2087
Yang K, Koike T, Yang D (2003) Surface flux parameterization in the Tibetan Plateau. Boundary-Layer Meteorol 106:245–262
Yang K, Koike T, Ishikawa H, Kim J, Li X, Wang J, Liu H, Liu S, Ma Y (2008) Turbulent flux transfer over bare-soil surfaces: characteristics and parameterization. J Appl Meteorol Climatol 47:276–290
Yang K, Qin J, Guo X, Zhou D, Ma Y (2009) Method development for estimating sensible heat flux over the Tibetan Plateau from CMA data. J Appl Meteorol Climatol 48:2474–2486